Benthic nitrate biogeochemistry affected by tidal modulation of Submarine Groundwater Discharge (SGD) through a sandy beach face, Ria Formosa, Southwestern Iberia

C. Rocha [a,*], J. Ibanhez [b], C. Leote [b,c]

[a] School of Natural Sciences, Trinity College, Dublin, Ireland
[b] School of Natural Sciences, Department of Geography, Trinity College, Dublin, Ireland
[c] Royal Netherlands Institute for Sea Research (Royal NIOZ), Department of Marine Chemistry and Geology, Texel, The Netherlands

ABSTRACT

To investigate both the role of tides on the timing and magnitude of Submarine Groundwater Discharge (SGD), and the effect on benthic nitrogen biogeochemistry of nitrate-enriched brackish water percolating upwards at the seepage face, we conducted a study of SGD rates measured simultaneously with seepage meters and mini-piezometers, combined with sets ($n = 39$) of high resolution in-situ porewater profiles describing NH_4^+, NO_3^-, $Si(OH)_4$ and salinity distribution with depth (0–20 cm). Sampling took place during two consecutive spring tidal cycles in four different months (November 2005, March, April and August 2006) at a backbarrier beach face in the Ria Formosa lagoon, southern Portugal. Our results show that the tide is one of the major agents controlling the timing and magnitude of SGD into the Ria Formosa. Intermittent pumping of brackish, nitrate-bearing water at the beach face through surface sediments changed both the magnitudes and depth distributions of porewater NH_4^+ and NO_3^- concentrations. The most significant changes in nitrate and ammonium concentrations were observed in near-surface sediment horizons coinciding with increased fraction of N in benthic organic matter, as shown by the organic C:N ratio. On the basis of mass balance calculations executed on available benthic profiles, providing ratios of net Ammonium Production Rate (APR) to Nitrate Reduction Rate (NRR), coupled to stoichiometric calculations based on the composition of organic matter, potential pathways of nitrogen transformation were speculated upon. Although the seepage face occasionally contributes to reduce the groundwater-borne DIN loading of the lagoon, mass balance analysis suggests that a relatively high proportion of the SGD-borne nitrogen flowing into the lagoon may be enhanced by nitrification at the shallow (1–3 cm) subsurface and modulated by dissimilatory nitrate reduction to ammonium (DNRA).

© 2009 Elsevier B.V. All rights reserved.

1. Introduction

Humans are now the greatest source ($140–190 \times 10^{12}$ g N year^{-1}) of fixed nitrogen (N) to Earths' ecosystems (Vitousek et al., 1997). Because most of this fixed nitrogen is being used in agriculture, the hydrological cycle tends to carry excesses as drainage or surface flow into the oceans. The nitrogen flux to the coastal zone has thus increased 9–10 fold since the mid 1920s (Mackenzie et al., 2002). But, in contrast with the relatively precise quantitative knowledge of N loading of the coastal ocean by surface flow or atmospheric deposition, very little is known about groundwater-borne nutrient inputs. Nonetheless, groundwater has been found to be a common transport route between land and sea for freshwater and associated land-derived nutrients, wherever the

hydraulic gradient on land is above mean sea-level and permeable paths connect continental aquifers to the seafloor (Johannes, 1980; Valiela, 1992; Valiela et al., 1992, 1999; Moore, 1999; Burnett et al., 2001, 2003; Bokuniewicz et al., 2003). Typically, a fraction of the freshwater flowing to the sea will discharge directly into coastal waters through a narrow seepage face on or in the vicinity of the intertidal zone (Bokuniewicz, 1992). The phenomenon is called Submarine Groundwater Discharge (SGD) by convention (Burnett et al., 2003).

However, permeable coastal sediments are also sites where pore water flow may be induced by other forces that overlap with the hydraulic gradients on land, including wave and tidal pumping (Ataie-Ashtiani et al., 2001; Burnett et al., 2003; Moore and Wilson, 2005). Hence, SGD often includes a varying, but usually large proportion of recirculated seawater (Taniguchi and Iwakawa, 2004). On the other hand, solutes carried by groundwater are likely subject to biogeochemical transformation while flowing seaward, both within the aquifer and at the seawater–freshwater mixing zone, including the seepage face (Moore, 1999; Charette et al., 2005; Charette and Sholkovitz, 2006). At

* Corresponding author. Tel.: +353 1 8963871.
E-mail addresses: rochac@tcd.ie (C. Rocha), pinoibaj@tcd.ie (J. Ibanhez), Catarina.Leote@nioz.nl, defreixc@tcd.ie (C. Leote).

the latter in particular, benthic loading of fresh marine organic matter and differential oxidant inputs promoted by advective processes, including convection, Bernoulli effects and wave and tidal pumping could potentially change the local biogeochemical reactivity (Uchiyama et al., 2000; Ullman et al., 2003), thus implying that the timing and extent of seawater recirculation through the freshwater–seawater mixing zone may play an important role in controlling nutrient exports from regional groundwater sources.

The complexity of the seepage face, brought by all the intersecting transport and reaction pathways mentioned above implies that quantifying SGD-borne contaminant loading into coastal ecosystems, as well as assessing the eventual mitigating role played by permeable sediments within the groundwater flow path and the subterranean estuary is a very complex task, explaining the lack of information thereof. Even so, reviews of existing data (Slomp and Van Cappellen, 2004; Moore, 2006) suggest that nutrient inputs to the coastal zone by SGD may rival riverine inputs at regional scales, thus promoting large, direct impacts on coastal ecosystems (Bowen et al., 2007). For example, the leaching of soils exposed to intensive agriculture, with an extensive use of fertilizers, has led to the increase of the phosphorus and nitrogen loads into coastal waters and a consequent enhancement of eutrophication, with subsequent impacts including the decline of coastal biodiversity (Capone and Bautista, 1985; Valiela et al., 1999; Paerl, 1999; Carruthers et al 2005; Verhoeven et al 2006).

Hence, the role played by benthic nitrogen reduction pathways, and in particular of denitrification, in attenuating nitrogen loading into coastal systems is important in the context of foreseen eutrophication pressure (Vitousek et al., 1997). Yet, our understanding of the nitrogen cycle seems to be heading for a major revision (Zehr and Ward, 2002; Hulth et al., 2005; Brandes et al., 2007). Alternative pathways for nitrate reduction, such as Dissimilatory Nitrate Reduction to Ammonium (DNRA), Anaerobic Ammonium Oxidation via nitrite reduction (Anammox) and Oxygen-Limited Autotrophic Nitrification–Denitrification (OLAND) have been found to occur alongside denitrification in overlapping sediment reaction zones (Dalsgaard and Thamdrup, 2002; Brandes et al., 2007). In opposition to denitrification and Anammox, and

to an unknown extent, OLAND, DNRA does not remove bioavailable N from the system. Although the relative role of these processes in coastal N processing is still largely unresolved, available evidence suggests that the main controlling factors over the expression of alternate nitrogen pathways in sediments are nitrate availability, the quantity and quality of available organic matter, and temperature (Herbert, 1999; Hulth et al., 2005). Because areas harbouring SGD may be the intersecting point of pelagic inputs of organic matter and major concentrations of inorganic compounds, including nitrate, seeping from the underlying strata, they may well host a potential plethora of overlapping nitrogen transformation rates and pathways. However, biogeochemical processes modulating nutrient loads carried into coastal waters by SGD remain critically understudied.

Here we examine temporal changes in benthic nitrogen biogeochemistry at a groundwater seepage face in a barrier island setting located in south Portugal. On the basis of measurements of seepage flow rates, nutrient concentrations and salinity in the outflowing water and on porewater nutrient concentration and salinity profiles acquired over successive tidal cycles, combined with ancillary evidence, we show that groundwater derived nitrate fluxes into the adjoining coastal waters depend on the tidal regime, are modulated by biogeochemical reaction fed by fresh marine organic matter, and explore, based on a local mass balance approach, the possibility of temporal and spatial overlap of nitrogen reduction processes at the seepage face.

2. Study area

2.1. Ria Formosa lagoon

The Ria Formosa, located in Southern Portugal (Fig. 1), is a leaky coastal lagoon system (Kjervfe, 1994) protected from the Atlantic Ocean by a multi-inlet barrier island cordon. Its present configuration consists of two peninsulas and five barrier islands, forming a sand dune cordon of ~80 km between Olhos-de-Água (Albufeira), to the West, and Vila Real de Santo António, near the border with Spain. The lagoon system has a surface area of ~111 km² with a maximum width of about 6 km in front
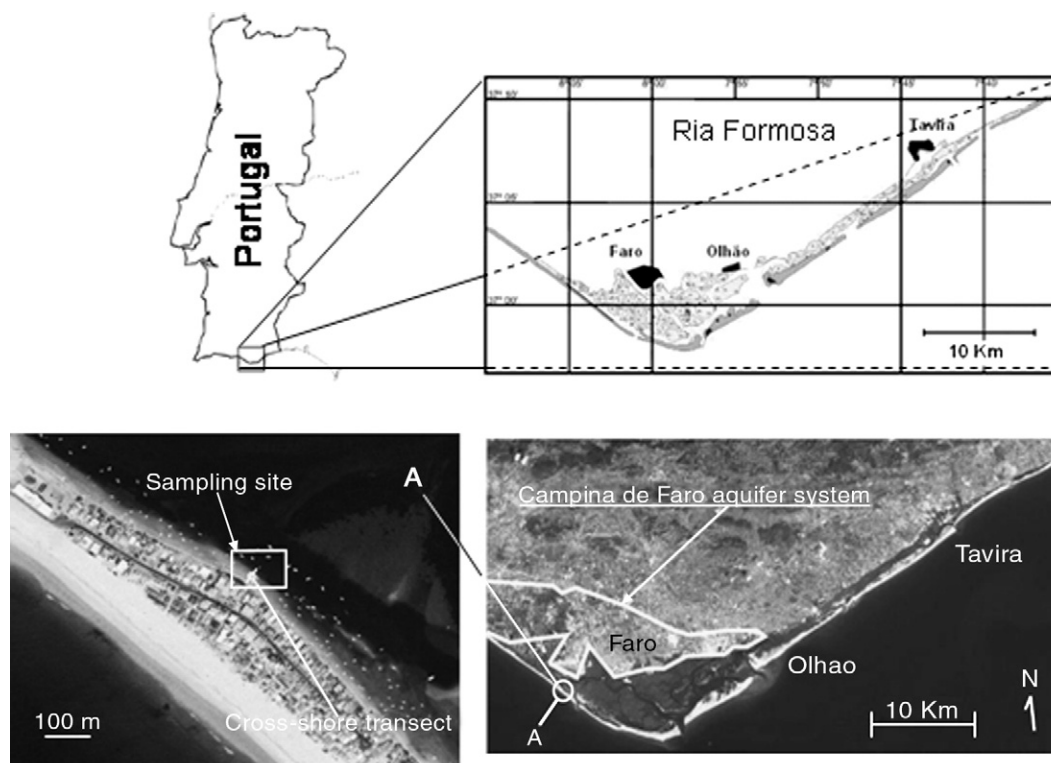

Fig. 1. Location of the sampling site in the Ria Formosa lagoon, southern Portugal.

of the city of Faro. The average depth relative to mean sea level is 2 m. The tide is semi-diurnal with average ranges of 2.8 m for spring tides and 1.3 m for neap tides. Occasionally, maximum ranges of 3.5 m can be observed during storm-surges (Vila-Concejo et al., 2004). The flooded surface during spring tides averages 86 km^2 but only 14% of this surface is permanently flooded whilst ~80% of the bottom emerges during spring low water (Andrade et al., 2004). The maximum tidal volume estimated by the Navy Hydrographical Institute (Hidrografico, 1986) is ~140×10^6 m^3. Lagoon waters are exchanged through five tidal inlets with the Atlantic ocean water-mass, with an average tidal prism of ~8×10^6 m^3 (Balouin, 2001). The renovation coefficient for the lagoon is 3.2 for spring tides and 1.0 for neap tides, translating to a very high (80 to 52%) daily water renovation capability. No significant surface fresh-water inputs exist (Andrade et al., 2004), which coupled to the high renovation capability, explains the average salinity of 35 found in the lagoon throughout the year.

The regional climate is semi-arid, with weak thermal amplitudes. Annual temperature average is 17 °C, with averages of 11 °C in winter and 24 °C in summer. The annual average precipitation at the city of Faro is 480 mm. The surrounding watershed covers 740 km^2, with an effective precipitation, after discounting the evaporative losses, of 152 mm per year, corresponding to a total average annual volume of ~1.2×10^6 m^3 (Salles, 2001), very small compared to the daily tidal exchange flux.

2.2. Geological and hydro-geological setting

The Campina de Faro, a coastal plain site of intensive agricultural activities lies directly North of the Ria Formosa's western sector. Since the early 80s, the original land cover of native oak and carob trees has been replaced by almond and olive trees and irrigated culture of citrus trees, tomato and vineyard. The ~50 m thick superficial aquifer system of the Campina de Faro (sands and gravels of the Plio-Quaternary) is connected through sub-horizontal Miocene sandy layers to under-lying Cretaceous limestones (Almeida et al., 2000), resting against a backdrop formed by the Serra massif (Pleistocene) and late Pleisto-cene unconsolidated sands (Chester and James, 1995). On the ocean side, the geological basement of the lagoon marshland is constituted by barrier platform sands roughly shaped into a prism by the slowdown of Relative Sea-Level Rise from 6000 BP (Bettencourt, 1994; Dias et al., 2000; Boski et al., 2002). It has an area of 86.4 km^2 (Almeida et al., 2000). Groundwater at the Campina de Faro has been intensively exploited both for irrigation and public water supply. In the late 80s, heavy nitrate contamination was detected in both the Quaternary and the Miocenic aquifer systems (Almeida and Silva, 1987), with average values of 1.7 mM ($n = 28$), and maximum values greater than 5.9 mM. Using the SO_4^{2-} to NO_3^{2-} ratio in the contaminated groundwater, Almeida and Silva (1987) showed that the source of contamination were inorganic fertilizers, which passed by direct infiltration into the topmost aquifer system and polluted the underlying Miocene sandy limestones by fluid interchange. Since the late 80s and early 90s (Stigter et al., 2006), several more controls have been carried out, in compliance with the EU nitrates directive; As a consequence, the Campina de Faro aquifer was designated a Nitrate Vulnerable Zone (NVZ) in 2001. By 2005, the NVZ of the Campina de Faro had been extended eastward, and a new one was created on the Campina da Luz aquifer (Bonte, 1999) system.

3. Methodology

3.1. Field sampling

3.1.1. Sampling strategy

In October 2005, sand fluidization was observed near the low water mark at the inner side of the western sand spit of the Ria Formosa (Fig. 1), along a strip of macroalgae (Ulva) growth. Infrared termography during low tide showed seepage of warmer ground-water against the colder intertidal background. These observations were subsequently compounded by a survey of the beach which revealed the brackish nature of porewater and water flowing through cross-shore runnels on the beachface during low tide.

Regular sampling of the site was initiated in November 2005. A series of 5 mini-piezometers (Turner, 1998), numbered from 0 to 4, and three in-situ acrylic profilers modified from the design of Seeberg-Elverfeldt et al. (2005), were deployed respectively cross-shore following the beach slope and along the low-intertidal beach profile (Fig. 2). Although both the sand fluidization and the macroalgae growth strip were observable along the whole inner extension of the sand spit, the sampling site (Fig. 1) was chosen based on convenience of access and existence of a nearby house that provided shelter during night sampling. Each profiler was buried in-situ with 12 Rhizon membrane samplers (Rhizon SMS-10 cm; Eijkelkamp Agriresearch Equipment, 0.1 μm pore size) located horizontally at vertical intervals of 1 (8 Rhizons up to 8 cm depth), 2.5 (3 Rhizons, respectively at 10, 12.5 and 15 cm depth) and 5 cm (1 Rhizon at 20 cm depth). Thus designed and deployed, the samplers provided the advantage of being left in place throughout the entire field experiment, causing minimal disturbance to porewater dynamics (Cappuyns et al., 2004). The soil moisture samplers were conditioned prior to deployment by flushing the membrane repeatedly with distilled water. Porewater profiles were taken at different time intervals albeit with increasing frequency during low tide, each month covering at least two consecutive ebb periods. Field sampling always took place during Spring tides. From January 2006 onwards, a series of Lee-type seepage flow meters (Lee, 1977), paired with miniature single point piezometers were also deployed at the site (Fig. 2, lower panel). With the exception of January, when the seepage meters were deployed in line with profiler A (Fig. 2), they were positioned in a rhomboid lineup with at least two chambers aligned with profiler B, with others either lower (profiler A) or higher (profiler C) in the beach profile, covering an area of roughly 7 m × 4.5 m. The single point piezometers were used to verify the fluxes measured with the Lee-type chambers, given the potential artifacts associated with their use (Cable et al., 1997). Water levels in the piezometers were verified regularly in parallel with seepage flux measurements. Across the beach profile, buried to a depth of 40 cm (50 for well 0), mini wells where deployed in lieu of the piezometers from November onwards, in order to assess the potential contribution of beach drainage to flow measured in the lower beach section. This study concentrated on two different sampling schedules, aiming to link porewater nutrient concentrations to temporal dynamics of SGD; In November 2005, the field experiment was designed to establish a temporal frame for sampling, one able to capture extremes in mixing regime within the first 20 cm of the sediment column as the tide level changed. The choice of time intervals over which to sample porewater concentration profiles was based on preliminary head data obtained prior to the sampling run in November 2005. Piezometer 4 (Fig. 2, lower panel) was sampled immediately following the beginning of active seepage during ebb tide. After converting measured head to vertical porewater velocity, results indicated that water started upwelling through the sediment at 0.17 cm min^{-1} and peaked at 0.57 cm min^{-1}, with an average of 0.4 cm min^{-1} during the ebb period. Flow at this velocity through the sediment pore space was capable of renovating the 20 cm length sediment column being sampled by the profilers in 117.6, 35.1 and 50 min, respectively. Because the objective was to capture the salient features of the predicted change in porewater distributions of salinity, nitrate and ammonium associated with the tide and SGD, the time intervals between profile samples were set lower than the more conservative estimates for water renovation times, thus allowing transient (i.e., non-steady state) profiles to be sampled. Thus sampling intervals (Fig. 6, upper panel) ranged from half hour (station A) to 3 h (station C). Sampling throughout 2006 would then be adjusted to the findings, in order to obtain porewater concentration profiles with minimum degrees of mixing (i.e. low salinity depth gradients). In this study, meter data from January, February, March and April are analysed
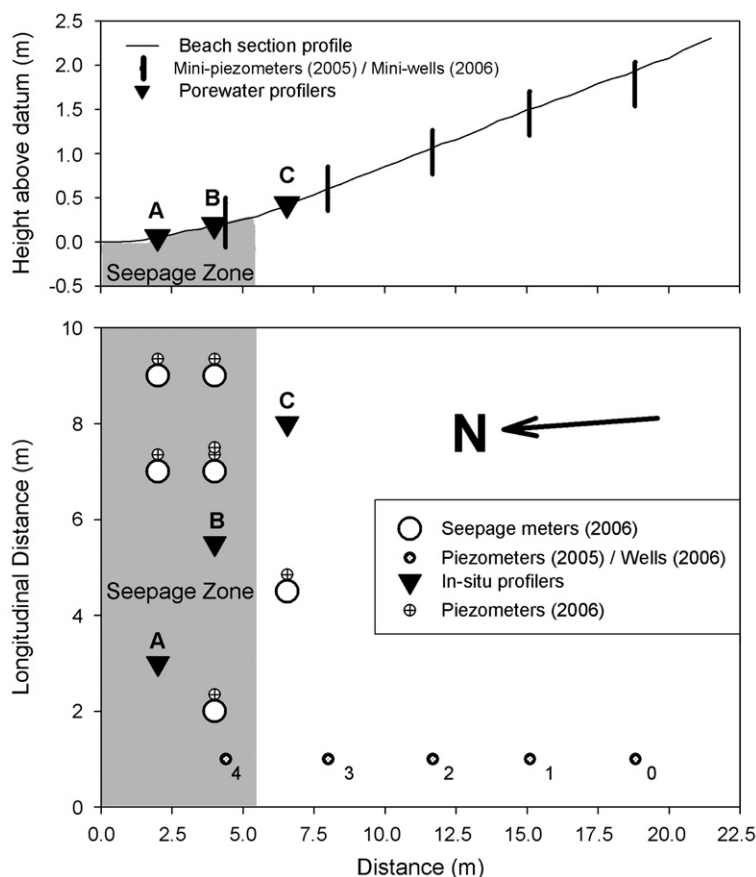
Fig. 2. Top: Beach profile with superimposed location of the porewater profilers (A, B, C) and either mini-piezometers (in 2005) or wells (throughout 2006) deployed to characterize beach drainage in a cross-shore transect (depicted by vertical bars at the appropriate locations). Mini-piezometers were used to measure porewater pressure within the beach along a cross-shore transect only in November 2005. All sampling done during 2006 employed mini-wells at the same positions, favouring the collection of water for chemical analysis (see Section 3.1.1. for more details of the sampling strategy), mini-piezometers being deployed next to the seepage chambers instead. Lower panel: View from above of the setup, according to the same cross-beach spatial scale.

in conjunction with porewater profiles from November 2005, March, April and August 2006 to establish the role of tidal height on mixing and reaction within the sediment column.

3.1.2. Porewater profiles of dissolved constituents

Pore water was collected in-situ into 11 mL vacuum flasks (BH Vaccutainer) via Luer-Lock ports mounted with a sterile syringe needle and connected to the sampling tubes protruding through the sediment water interface above the acrylic profilers. The first extracted millilitre, corresponding to the dead volume inside the tubing, was discarded (Seeberg-Elverfeldt et al., 2005). Porewater aliquots intended for chemical analysis (5–6 ml from each depth, sealed inside the vacuum tubes), were then stored at 4 °C until laboratory processing. Porewater samples collected in this manner do not require further preserving agents (Luo et al., 2003; Song et al., 2003; Seeberg-Elverfeldt et al., 2005). All analytical work was completed within 2 weeks of sampling. Additional samples from the overlying water column were taken with a single membrane sampler, connected to a vaccutainer left to float over the sampling transect while filling (10 mL).

3.1.3. Seepage measurements

To measure SGD fluxes, four to seven manual seepage meters were deployed during low tide (Leote et al., 2008). Sampling started during the subsequent ebb period, following the precautions suggested by Cable et al. (1997), and carried on for a minimum of two consecutive tidal cycles (see Fig. 5). Plastic collection bags were

connected to the chambers by transparent polypropylene tubing with a cross-section of 0.6 cm. The volume of water in the bags was registered throughout the sampling period, with an occasional sample (~7 mL) taken for nutrient analysis by direct suction through a Rhizon membrane into a vaccutainer flask. Salinity, pH and oxidation–reduction potential (ORP) was measured in the bag water samples on-site using an YSI 600 (Yellowspring Instruments) multi-parameter probe. There was no predetermined sampling interval, for logistical reasons. Each chamber had two plastic bags attached to independent outlets to minimize the random possibility of flow lines being clogged. A total of 8–14 plastic bags were thus deployed for three consecutive tidal cycles, which made the human effort of controlling all of them in regular time intervals almost impossible given the high flow-rates during low tide periods. Instead, bags were sampled when they were almost full, on a bag-by-bag basis, and the timing of samples noted.

3.1.4. Sediment properties

Bulk sediment properties (water content, porosity, organic content) were determined in three replicate (30 cm long, 4.5 cm Ø) cores taken between the upper and lower chamber line, each set aligned with the position of the porewater profilers (A, B and C). Extra core samples (10 cm length, 3.5 cm diameter) were taken by hand at two locations on the low-intertidal beach profile (in between the porewater profiler locations, Fig. 2) for more detailed profiling of hydraulic conductivity. Further cores were taken at the end of the field sampling program, sealed
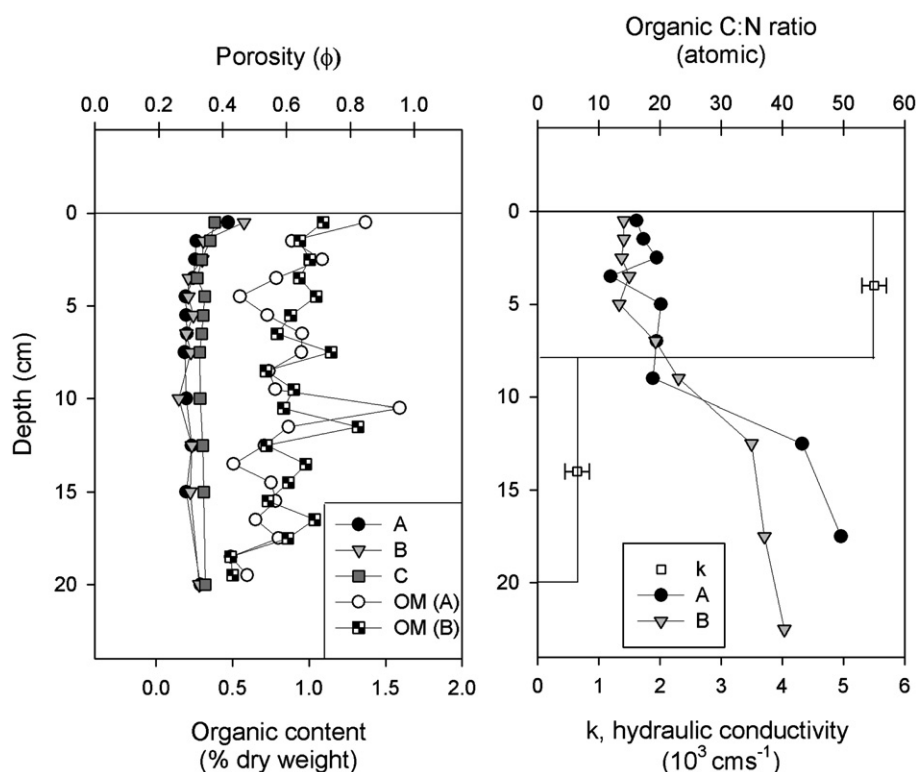
Fig. 3. Left: Depth profiles of organic matter content (OM (A) and OM (B) in plot legend) and porosity (A, B, C in plot legend) for the sediment column at the A, B and C beach levels, in alignment with the position of the porewater profilers. Note horizontal (*X*-axis) scaling out of phase with each other, to avoid overlap of the two plotted series. Right: Combined plot of the hydraulic conductivity in two sub layers of the sediment and the depth gradient of organic matter composition, represented by the bulk organic C:N ratio. Error bars on the hydraulic conductivity plots represent the S.E. of the average of 8 measurements.

inside the respective core-liners with rubber stoppers and latex sealing tape and transported vertically to the lab for the determination of elemental composition of the organic matter.

3.2. Analytical methods

3.2.1. Water solute analysis

The pore water, mini-well and overlying water samples were analyzed for NO_3^-, NO_2^-, NH_4^+, $Si(OH)_4$ and salinity. Nutrient analysis (NO_2^-, NH_4^+ and $Si(OH)_4$) was performed following laboratory protocols based on Grasshoff et al. (1999) previously adapted to low (0.5 mL) aliquot volumes. NO_3^- was quantified following the spongy cadmium method (Jones, 1984). DIN was calculated as the sum of NO_3^-, NO_2^- and NH_4^+ concentrations. Porewater salinity was measured by hand-held refractometer on the remains of the porewater samples, after results from all other analysis were confirmed by replication.

3.2.2. Whole sediment analysis

Long cores were sliced and sequentially sieved to determine the percent contribution of very coarse sand (1–2 mm), coarse sand (0.5–1 mm), medium sand (0.25–0.5 mm), fine sand (0.063–0.250 mm) and silt + clay (<0.063 mm) according to the Udden-Wentworth scale (Wentworth, 1922). Cumulative weight percentage plots were used to determine the median grain size at the 50th percentile. Total C and N were measured in a Carlo Erba CHNS A1108 elemental analyzer following Hirota and Szyper (1975), before and after elimination of carbonates by acidification with HCl. Water content was determined in each sub-sample as a percentage of weight loss at 60 °C after 24 h and total organic matter content was quantified as the percent weight loss after ignition (450 °C, 4 h). Porosity was calculated based on the water content, using 2.65 g ml^{-1} (quartz) as the dry sediment density.

Hydraulic conductivity was measured in separate cores by falling-head permeametry, and horizontal and vertical permeability derived from the data by the method described in Rocha et al. (2005).

4. Results

4.1. Beach face characterization

The sediment at the site was classified as medium sand with a median grain-size (d_{50}) of 0.44 mm, and low clay + silt content by weight (1.6% at station A and 0.08% at station B). The porosity (Fig. 3, left panel), changed little with depth, with a slight maximum of 0.38–0.42 at the surface layer, and averaged 0.31 ± 0.04, 0.32 ± 0.05 and 0.34 ± 0.02 over the 20 cm-deep sampled sediment column for sites A, B and C, respectively. Hydraulic conductivity averaged $5.5 ± 0.2 × 10^{-3}$ cm s^{-1} (n = 8) over the surface 8 cm layer, while the 12 cm layer beneath had a lower conductivity of $6.5 ± 2 × 10^{-4}$ cm s^{-1} (n = 8). The effective hydraulic conductivity over the first 20 cm depth for vertical porewater flow was $1 × 10^{-3}$ cm s^{-1} (Cardwell and Parsons, 1945). Total organic content ranged from 1.37% of dry weight at the surface (Station A) to 0.49–0.6% at 20 cm depth, generally decreasing with depth, but showing subsurface peaks between 10 and 12 cm (1.59% at site A and 1.32% at site B). These coincided with the sediment horizon where a drop in hydraulic conductivity was evident (Fig. 3, right). Total Organic Carbon (TOC) decreased from 0.98–1.22% at the surface to 0.8–0.5% at 20 cm depth, with isolated peaks visible between 6 and 8 cm depth (1.15% station A and 1.1% station B). The distribution of the atomic C:N ratio suggested that organic matter quality was divided in three different layers with depth (Fig. 3): for station A, a slight impoverishment in N was observed (C:N from 16 to 20) down to 7.5–9.5 cm depth, whilst below that, following a transitional layer, N impoverishment was clear (C:N of 43–49.6). The change in C:N ratios with depth was more regular at site B: an

almost constant ratio of 13–14 was measured down to 5 cm depth, while from there to 12.5 cm depth the ratio increased linearly to ~34. Below the 12.5 cm layer, the C:N ratio steadily increased from 35 to 40.

The mini-wells deployed along the beach slope (Fig. 4) were used to verify the level, nutrient composition and salinity of the water table beneath the beach face, particularly upstream of the seepage zone. Nitrate concentrations, plotted against salinity, showed that the water in the wells could be differentiated between highly saline (>36) and low nitrate content (upper beach face, Well 1) and brackish (<36) water with increasing nitrate contents (downslope, to Well 4). Located at the active seepage face (Fig. 2, lower panel), the latter showed some distinctive features. Water was always present in the well throughout ebb periods, something not observed in others, and nitrate levels were always the highest (above 10 µmol L^{-1}) whilst salinity was lowest.

4.2. Temporal variability of SGD

Seepage followed a regular pattern, inversely correlated with tide levels as shown by both seepage meter and piezometer data (Fig. 5). In order to be directly comparable to seepage flux measurements, piezometer head readings were converted to flux using Darcy's law and the cross-sectional area covered by the meters (0.11 m^2). Discharge during high tide was always quite low, averaging 2.2 ($n=6$), 2.44 ($n=5$), 2.66 ($n=8$) and 4.08 ($n=8$) cm^3 min^{-1} in January, February, March and April, respectively (Fig. 5). High seepage rates were observed during low tide with both chambers and piezometers, although chamber fluxes peaked less regularly than piezometer-derived equivalents (e.g., February, 2nd ebb period). In order to obtain a maximum discharge figure for each month, seepage rates above the 75th percentile of each dataset were averaged (±standard error), to give 57.5 ± 9.1 ($n=9$) in January, 53.6 ± 7.1

Fig. 4. Nitrate concentrations measured in water samples collected from the mini-wells deployed along the beach profile, plotted against salinity. Well identification numbers increase downslope. See also Fig. 2.

($n=8$) in February, 109.4 ± 7.2 ($n=14$) in March and 109.8 ± 13.5 ($n=10$) cm^3 min^{-1} in April. In similar fashion, the highest piezometer-derived fluxes averaged 64.6 ± 5.4 ($n=14$) in January, 104.5 ± 5.1 ($n=10$) in February, 135.2 ± 2.5 ($n=19$) in March and 129.4 ± 7.5 ($n=6$) cm^3 min^{-1} in April.

4.3. Benthic profiles of NH_4^+, NO_3^- and $Si(OH)_4$ at the seepage face

Porewater NO_3^- and NH_4^+ concentration profiles collected through three successive low tide periods are compared to the porewater salinity gradients on the lower panels of Fig. 6. At station C, analyte concentrations do not change with depth or time, confirming that at this location, the porewater composition probably only reflects upper beach drainage. This observation was consistent throughout the other months (data not shown). Salinity (median 39.5, average 39.4 ± 0.48, $n=62$) was higher than that of mean seawater throughout the 20 cm depth sediment layer, while concentrations of NO_3^- and NH_4^+ averaged 2 and 0.85 µmol L^{-1}, respectively (Fig. 6, lower panel). In contrast, brackish groundwater discharge affected the porewater distributions of NO_3^- and NH_4^+ at positions A and B. There, porewater analyte concentrations and depth gradients changed in response to active seepage, and thus varied with tidal stage (Fig. 6, middle panels). NH_4^+ concentrations were lowest at 20 cm depth at both sites, but increased sharply in the direction of the surface, above 15 cm depth. Two subsurface peaks were measured throughout the sampling period (median concentrations ~5–7 µmol dm^{-3} bulk sediment at A and ~10 µmol dm^{-3} bulk sediment at B). No significant correlation was found between NH_4^+ and salinity at site B, although at A, there was a positive correlation between these two parameters (Pearson product moment correlation = 0.329, $P<0.005$, $n=72$). Conversely, NO_3^- concentrations oscillated at depth in opposition to salinity and tide level. Lower salinity (25–30) was significantly correlated with higher NO_3^- concentrations (>10 µmol dm^{-3} bulk sediment), as confirmed by Pearson product moment analysis (for A: correlation coefficient = −0.395, $P<0.001$, $n=72$; and for B: correlation coefficient = −0.514, $P<1×10^{-6}$, $n=72$). Nitrate levels decreased rapidly towards the sediment surface, reaching 1–2 µmol dm^{-3} between 10 and 0.5 cm depth (site B) and 10 to 5 cm depth (site A). Subsurface peaks observed in NO_3^- distributions where visually complementary to NH_4^+ minima, and vice versa, on 8 out of the 12 profiles. This visual understanding was confirmed by a strong negative correlation found between NO_3^- and NH_4^+ concentrations on the whole dataset collected at sites A and B (Pearson Product Moment correlation, A: Correlation coefficient = −0.353, $P<0.005$, $n=72$; B: Correlation coefficient = −0.461, $P<0.0001$, $n=72$). The outstanding 4 profiles (sets A2, A5 and B2, B5, Fig. 6), were taken prior to or at the moment seepage started.

A selection of profiles obtained in March and April are plotted in Fig. 7. These are complemented with additional profiles sampled in August (Fig. 8), in order to compare NO_3^- and NH_4^+ porewater distributions at low tide, when seepage was very active, to profiles representative of no significant seepage, taken at peak high tide. In general, salinity profiles were regular throughout the sediment column, and maintained coherence with tidal stage throughout the tidal cycle (i.e., same tidal stage, similar salinity profile). However, NH_4^+ concentrations were not at the same level as in November. NH_4^+ concentrations were only relevant at station B, in March, and only for two of the sampled profiles, one taken at the very beginning of active seepage (21:35, salinity 35–36 throughout the sediment column) and one at the end of the seepage period (13:10, salinity ~25 throughout the sediment column). Both were sampled while the site was still flooded. Nevertheless, when ammonium was present, profile shape was similar to the median found in November (Fig. 6, middle panels), with subsurface peaks in the uppermost layers. Sediment porewaters were almost entirely devoid of NH_4^+ at the time all the other profiles were sampled, including those in August (data not shown). By contrast, nitrate was always present in the porewater when seepage
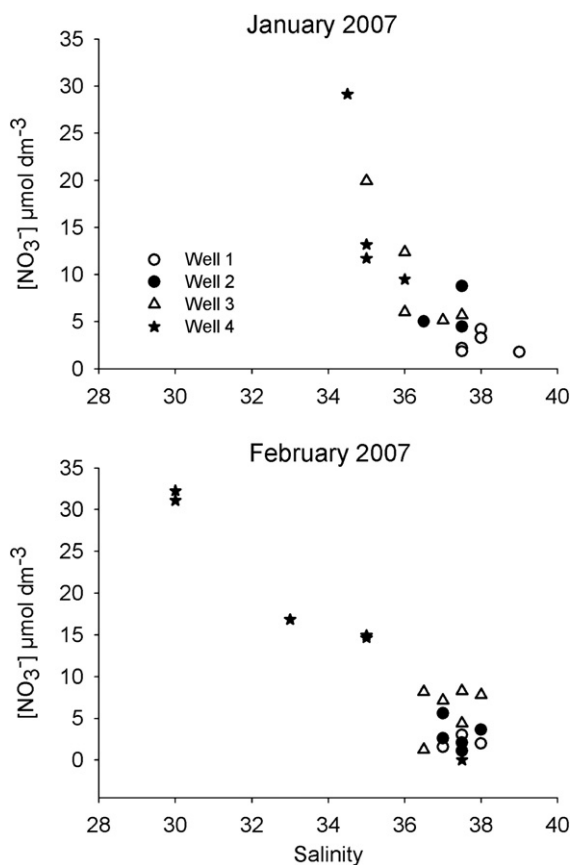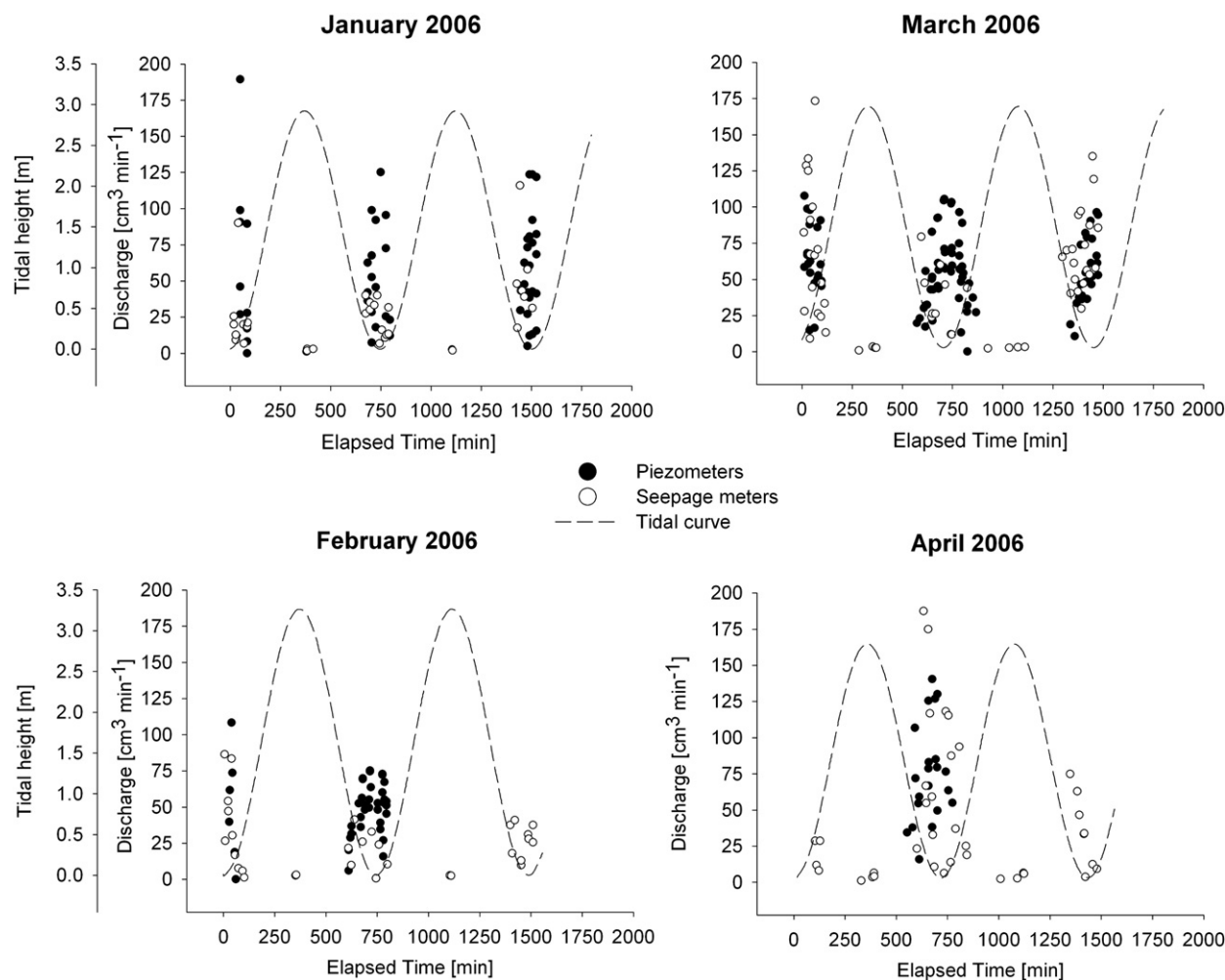
January 2006

March 2006

February 2006

April 2006

● Piezometers
○ Seepage meters
- - - Tidal curve

Fig. 5. Tidal variation of groundwater discharge through the beach face, measured in parallel with seepage meters (0.11 m² area each) and mini-piezometers for greater reliability. All data collected during at least 2 consequent tidal cycles in January, February, March and April 2006 is plotted.

was active (Figs. 7 and 8), although concentrations at the deeper layers where lower than those found in November (Fig. 6). Also, nitrate was present throughout the whole sediment column, albeit oscillating in opposition to salinity as before, particularly at site B. However, the most salient feature of NO_3^- depth distributions in March, April and August was a near-surface peak maintained against large seepage rates. Concavity in the deeper gradients was also less marked than in November, when the sampling strategy aimed for a time-series analysis of the system.

The highest nitrate concentrations where always found near the surface: 20 μmol dm^{-3} bulk in March (A) and ~6 μmol dm^{-3} bulk in April, for depth-averaged salinities of ~20–23 and ~25 (March A and B respectively) and ~30 in April (A). During high tide (no seepage, salinity ~35) in August (Fig. 8), the sampled sediment column was devoid of nitrate up to 20 cm depth, at odds with the profiles sampled under active seepage, when peaks of ~40–45 μmol dm^{-3} bulk were observed near the surface and the asymptotic concentration levels ranged from ~28 (A) to 10 μmol dm^{-3} bulk (B). Ammonium was not detected in August, even at low tide (data not shown).

5. Discussion

5.1. Temporal variation of SGD

Seepage meter data (Section 4.2, Fig. 5) shows that SGD peaks in phase with low tide. However, seepage meters are somewhat unreliable in precisely quantifying SGD (Shaw and Prepas, 1989; Cable et al., 1997),

in spite of still being the simplest to operate and the sole devices allowing parallel quantification of flow rates and seepage water composition. However, the potential artifacts mentioned by Shaw and Prepas (1989) become less determinant of data quality when high seepage rates are measured (Cable et al., 1997), as in our case (Leote et al., 2008). Even so, mini-piezometers deployed alongside the meters provided independent head data allowing a measure of control for the chamber-measured flow rates and temporal variability (Fig. 5). Piezo-meter derived data (Fig. 5, Section 4.2), suggested that seepage meters might be underestimating peak flow rates in February and March. Heterocedastic t-tests comparing the means of 75th percentile flow rates by both methods (the null hypothesis was that there were no significant differences between them) showed that peak flow rates measured by chambers with a 0.11 m² area (53.6 ± 7.1 cm³ min^{-1}, $n = 8$, and 109.4 ± 7.2 cm³ min^{-1}, $n = 14$, respectively) were significantly lower (null hypothesis rejected with $P = 3 \times 10^{-5}$ and $P = 0.0019$, for February and March, respectively) than those obtained from head data (104.5 ± 5.1 cm³ min^{-1}, $n = 10$, and 135.2 ± 2.5 cm³ min^{-1}, $n = 19$). In January and April, by contrast, no significant difference was found between peak flow rates determined by the two methods. However, both methods showed that SGD peak rates were in phase with low tide (Fig. 5). Also, we observed that there was no substantial phase lag between sites A, B and C (see piezometer-derived curves, Fig. 5).

By using salinity as an inert tracer for the degree of mixing in the water collected from the seepage meters, we calculated the relative proportion of freshwater present in the SGD samples (Fig. 9). Our results show that the relative contribution of the freshwater
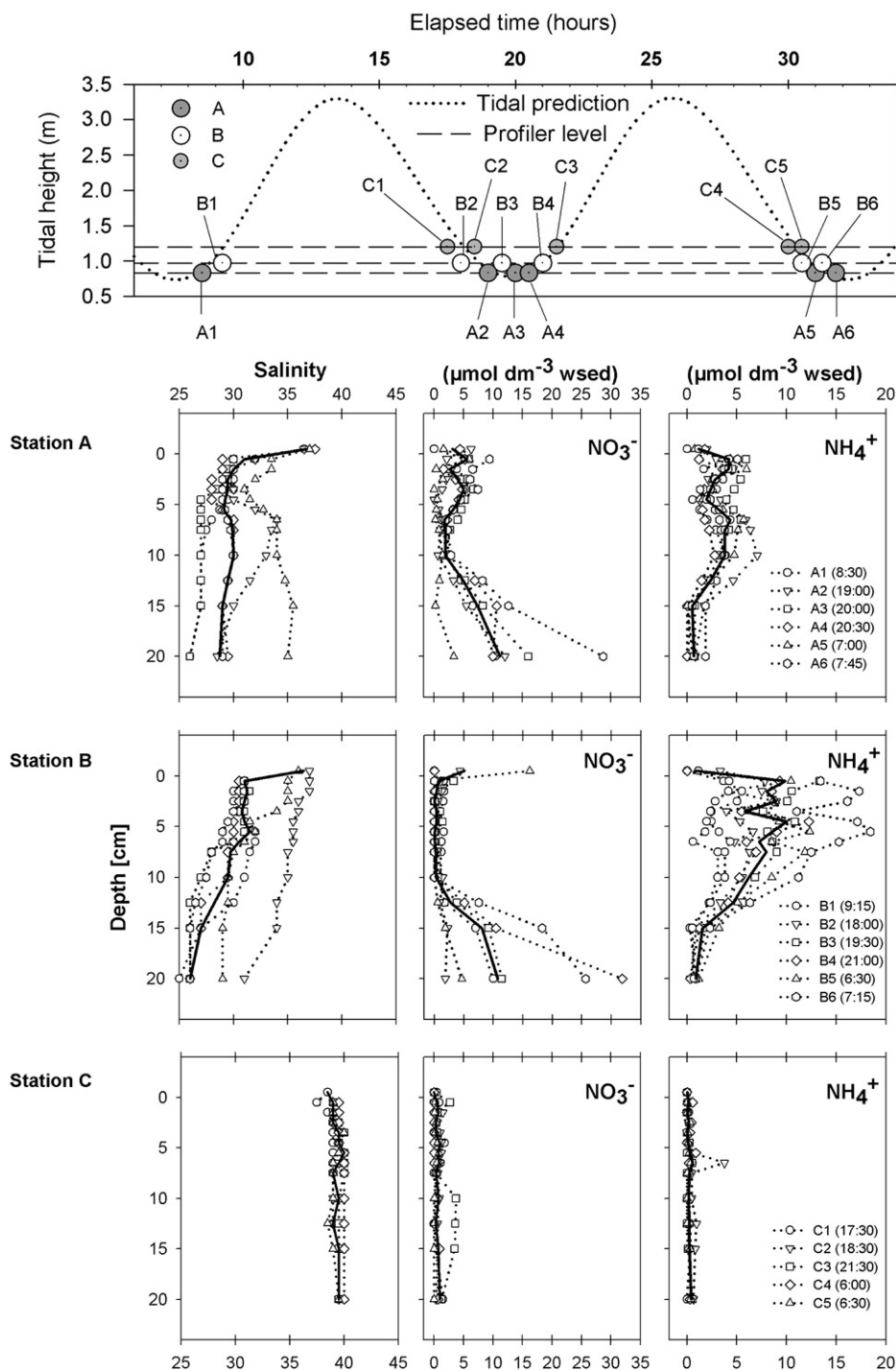
Fig. 6. First panel, top: timing of sampled profiles with respect to the actual tide level at the site during the sampling period. The relative position of each profiler (A, B and C) at the beach face is referenced by its elevation above the lowest low water mark (vertical axis scale) — a dashed horizontal line (time line) therefore runs through all the in-situ profiles at a certain position on the beach face. Lower panels: profiles depicting the variation of porewater levels of NO_3^-, NH_4^+ and salinity with depth for November 2005, respectively for positions A, B and C at the beach face. Number suffixes for each letter refer to the temporal sequence of profiles obtained throughout the tidal cycle (see top panel). Solid lines depict the median of the concentration at each depth. Dotted lines represent individual profiles, to allow assessment of the range in variation measured throughout the sampling period.

component of SGD was also in phase with the low tide, thus implying that the hydraulic gradient on land driving SGD was augmented when sea level decreased with the tide in the lagoon, and therefore that the tide is a major factor controlling the temporal dynamics of SGD at our site. This is in agreement with results obtained elsewhere (Robinson et al., 1998; Robinson and Gallagher, 1999; Taniguchi, 2002; Taniguchi et al., 2003; Urish and Mckenna, 2004). Apart from the tidal amplitude, the mean neap-spring tide oscillation has also been related to the recharge of saline water into the mixing zone, thus

suggesting that it might control the amount of recirculated SGD, as shown in Osaka Bay, Japan (Taniguchi, 2002). However, seepage flux oscillation and tidal amplitude are not always in phase, because the extent of the phase lag depends primarily on the local hydrogeo-morphology (Urish and Mckenna, 2004; Paulsen et al., 2004). Given the morphogeographic context of the Ria Formosa, the forces underpinning pressure gradients driving seepage rates at our site (Fig. 5) have to be discussed according to three main threads of reasoning: firstly, the land-based piezometric surface on the coast
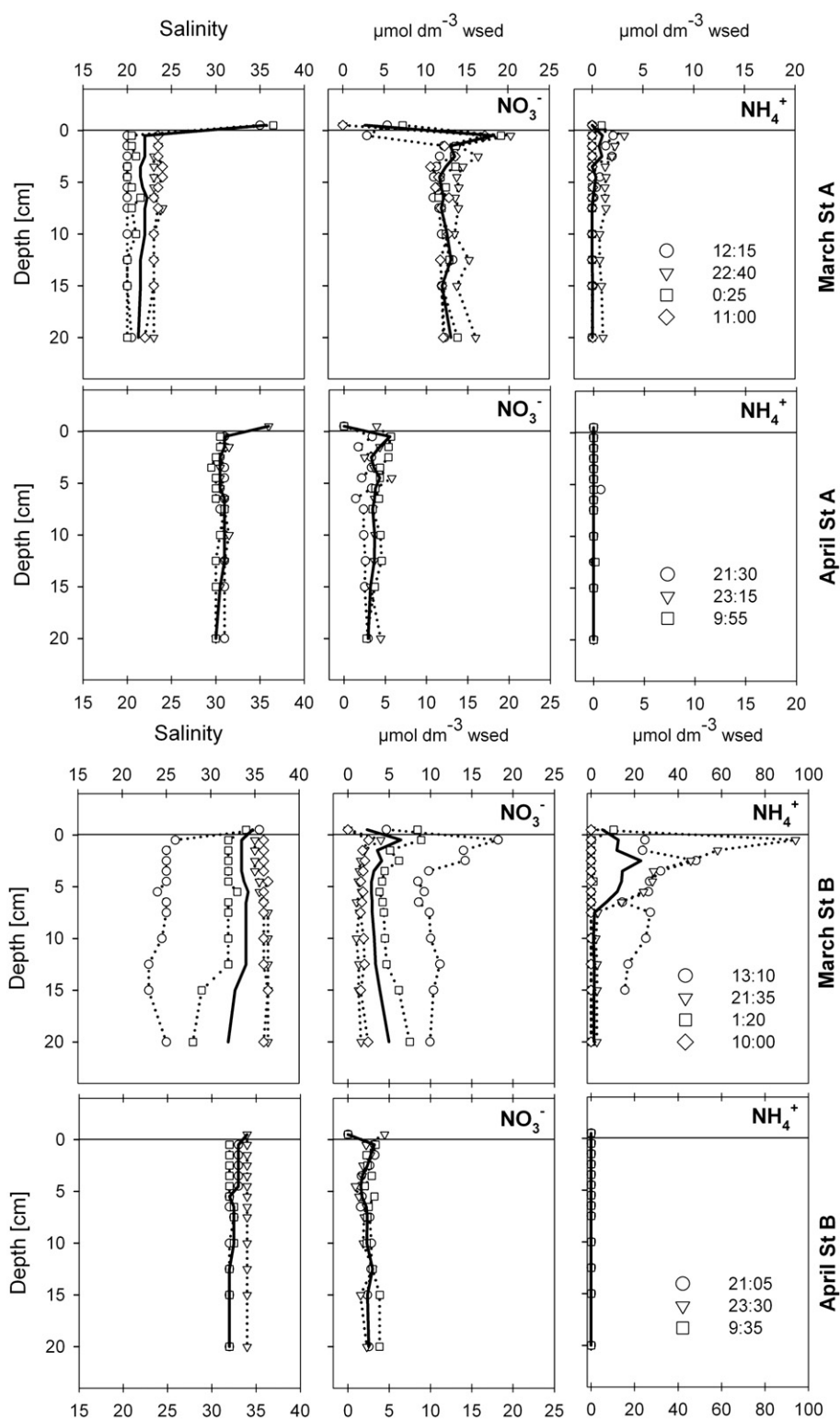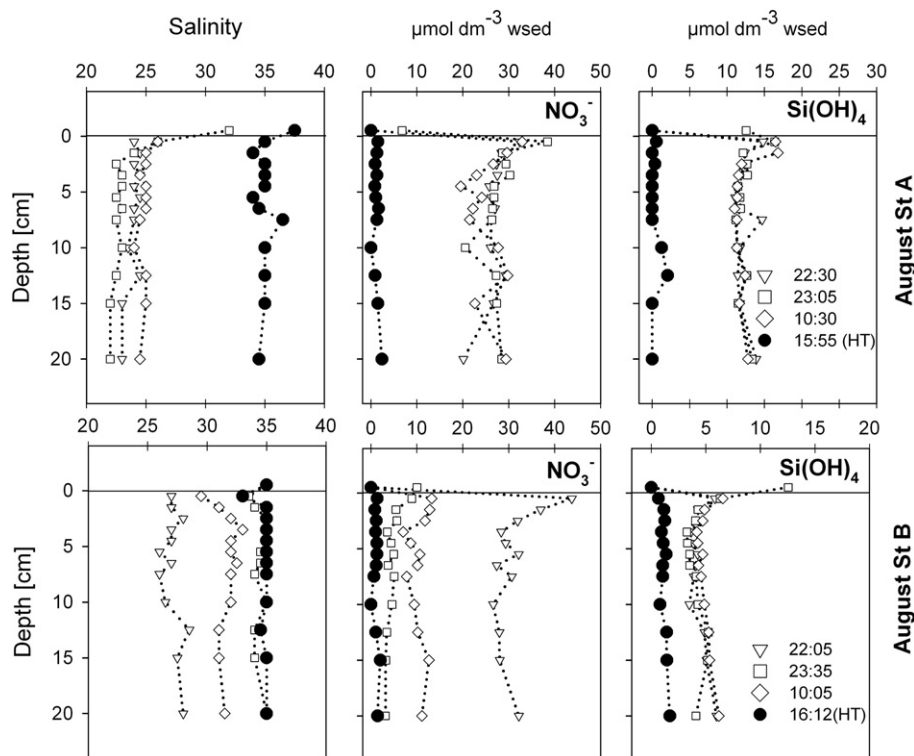
Fig. 7. Profiles depicting the concomitant variation of porewater levels of NO_3^-, NH_4^+ and salinity with depth for March and April 2006 during two consecutive low tide periods, at two positions in the beach (A: lower end of the seepage zone; B: upper limit of the seepage zone). Timing is in sequence, i.e., the first plot in each graph is the first profile sampled at the site, and so consecutively on. Solid lines depict the median of the concentration at each depth. Dotted lines represent individual profiles, to allow assessment of the range in variation measured throughout the sampling period.

and the resulting hydraulic gradient into the lagoon; secondly, the possibility of tidal pumping of groundwater across the barrier island cordon, shown to be important, for example, in Florida Bay (Chanton et al., 2003); and finally, by contextualizing these forces against the backdrop of the precipitation regime and the Ria Formosa tidal prism.

### 5.2. Influence of the tide over local forces driving SGD

The stratigraphic evidence suggests that the infilling sequence is quite uniform throughout the lagoon (Bettencourt, 1994). Muddy layers, 0.60 to 1.3 m thick, cover Quaternary gravels and sands throughout the lagoon (Arnaud-Fassetta et al., 2006). The thickness of

Fig. 8. Profiles depicting the variation of porewater levels of NO_3^-, $Si(OH)_4$ and salinity with depth for August 2006 during two consecutive low tide periods, at two positions in the beach (A: lower end of the seepage zone; B: upper limit of the seepage zone), compared to profiles taken at high tide (HT) from the same profilers using SCUBA diving.

this infilling sequence varies from 5–8 m minimum at the continental fringe to about 30–50 m below the barrier island cordon (Bettencourt, 1994). Stratigraphic transects through the western flank of the Ancão peninsula, where our sampling took place, confirm the connection between the barrier island cordon and the sands and gravels underlying the backbarrier marshes (Arnaud-Fassetta et al., 2006).

To the east of our site and north of the recently opened Ancão inlet (Fig. 1), the subsurficial sandy sediments were shown to host diatom assemblages tolerant of brackish/freshwater conditions and to be devoid of foraminifera (Andrade et al., 2004), suggesting a contemporary freshwater table. Hence, the ancillary evidence strongly supports the assertion whereby the continental aquifer ensemble
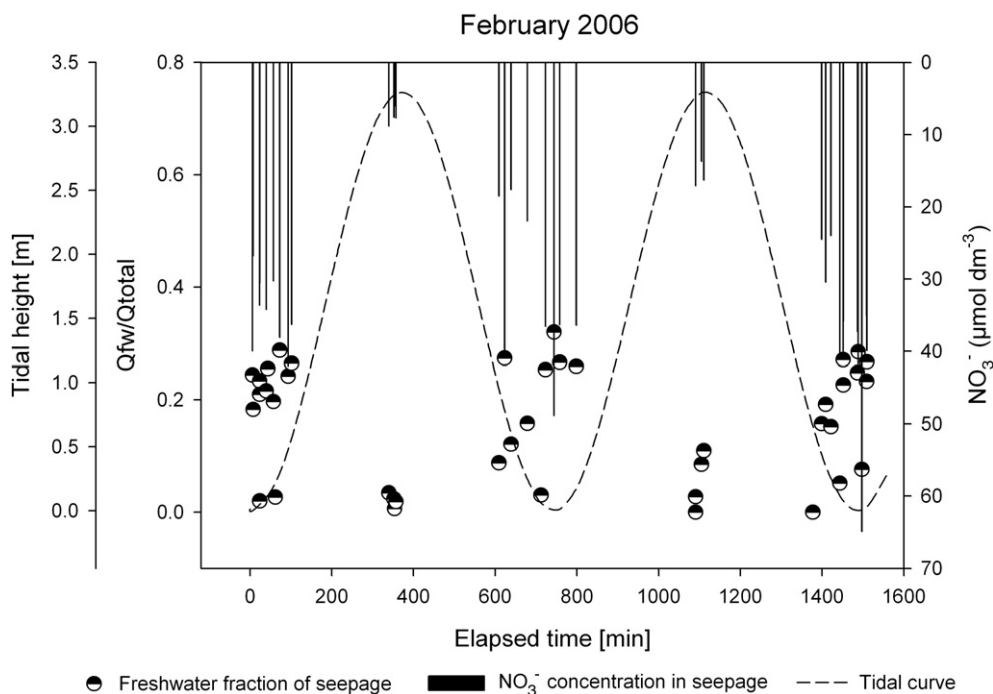
Fig. 9. Relative proportion of freshwater present in SGD collected by the seepage meters, plotted as the ratio between total freshwater volumes to total seeped volume (Qfw/Qtot), for the sampling period covering two consecutive tidal cycles in February 2006, compared with the concentration of NO_3^- measured in the discharged water (note inverted scale on the right hand side axis) and to the tidal level.

extends below the Ria Formosa and into the barrier island cordon. Finer sediments sustaining the marshland act as a confining layer for subsurface flow, in a geomorphological context reminiscent of typical saltmarsh ecosystems (e.g. Charette, 2007). Continental groundwater may flow below this confining layer, seeping to the surface only through the coarse sediments lining the bottom of natural tidal creeks and dredged channels, backbarrier beaches and intertidal sandflats, local hydraulic gradient permitting (Johannes, 1980; Corbett et al., 1999), which is the case: groundwater in the Campina de Faro aquifer flows from North to South (Stigter et al., 1998). The head above Mean Sea Level (MSL) at the continental fringe north of our site, taken from piezometric data on 15 boreholes (SNIRH/INAG, 2008) was 2.98 m for the 2005/2006 water year. Therefore, the hydraulic gradient from the mainland to our site was on average 0.0006 to MSL. Because the largest tidal amplitude is ±1.75 m, the gradient will increase to 0.0012 during spring low water and decrease to -0.1×10^{-5} at spring high water (permitting recharge). Thus the tide may indeed be a major force defining both the timing and magnitude of SGD.

The lower limit of the marshland starts between 1.70 and 1.80 m, slightly below mid-tide level (1.93 m), according to recent measurements in the western flank (Arnaud-Fassetta et al 2006). In combination with the stratigraphical evidence, this fact suggests that the underlying permeable sediments in contact with the continental aquifer, including the sandy intertidal, tidal creeks and meanders and the backbarrier beach faces start at MSL or below. Hence, pressure variations controlling SGD in these areas, driven by the hydraulic gradient established between land and lagoon will be higher when tidal level decreases below MSL, a decrease that is highest during Spring tides. Our results accordingly show that the freshwater component of SGD increases from mid-tide level to low tide, decreasing again with the rising tide, in phase with the total discharge rates (Fig. 9).

Cross barrier tidal pumping might also be modulating SGD (Bokuniewicz and Pavlik, 1999; Chanton et al., 2003). Prior to the reopening of the Ancão inlet, the maximum difference between the Atlantic tidal height and the tide level within the lagoon was 0.11 m during spring tides (Seabra de Melo, 1989). The width of the barrier island at our location is ~250 m (Fig. 1). Under the idealized conditions mentioned above (0.11 m maximum difference) a gradient of 0.00044, lower than the land–ocean hydraulic gradient to MSL, would exist. However, since the new inlet established itself, lagoon-sea exchange has increased (Vila-Concejo et al., 2003) reducing the tidal height difference significantly, thus minimizing the relative role played by cross-barrier pumping.

The fact that the tidal prism is 6.7 times greater than the annual precipitation over the entire drainage basin, immediately suggests that the composition of SGD within the lagoon might be dominated by recirculated marine water, which was confirmed on an annual basis (Leote et al., 2008). The freshwater component of seepage flow averages ~30% annually, during spring tides (see also Fig. 9). The tide level effect on the land–ocean hydraulic gradient and the relatively high percentage of freshwater observed during our study suggests that the fresh to recirculated seawater ratio in SGD peaks during spring low tides and will decrease from spring to neap tides.

5.3. Effect of SGD pulses on nitrate biogeochemistry at the seepage face

Previous work showed a very strong inverse correlation between salinity and nitrate levels in the groundwater seeping from the beach face, indicating that porewater nitrate is mainly sourced from continental freshwater (Leote et al., 2008). Nitrate concentration at 20 cm depth at the seepage face accordingly oscillates in opposition to tide level (see Section 4.2 for statistical validation), and in phase with the freshwater component of SGD (Fig. 9). The time series of pore-water concentration profiles collected in November 2005 (Fig. 6) shows that NO_3^- is pumped into the 20 cm deep superficial layer from

below, and advected to the surface by the upwelling mass of brackish water when the pressure head induced by the overlying water decreases. As the tide recedes, salinity at 20 cm depth decreases and nitrate concentrations increase (Fig. 6, profiles 2, 3, 4, in sequence, then 5, 6). When mounting levels of nitrate are pumped into the overlying sediment layers, a rise in ammonium concentrations is observed closer to the surface (Fig. 6) at a depth where nitrate levels decrease again (0–10 cm). Additional evidence relating tidal stage to the benthic biogeochemistry of nitrogen may be gathered from the sets of NO_3^- and $Si(OH)_4$ porewater profiles taken during low tide and compared to depth distributions measured at high tide (Fig. 8). Silicate does not participate directly in benthic oxidation–reduction reactions, but is often present in high concentrations in coastal groundwater (Kim et al., 2005). Profiles taken in August show a clear difference both in porewater levels and concentration gradients between low tide (active seepage) and high tide (none or residual seepage). Porewater silicate levels are consistently higher during active seepage than in the absence of SGD, i.e., during high tide, in similar fashion to nitrate (Fig. 8). In addition, no significant differences in inter-profile variance or depth gradients are evident when SGD is active. On the other hand, nitrate profiles change with overall porewater salinity (August B, Fig. 8), suggesting that observed changes in NO_3^- concentration are not merely an artefact of mixing and therefore indicating that the seepage process affects benthic redox reactions.

Sediment layers where the most significant changes in nitrate and ammonium concentrations are observed (Figs. 6–8) coincide with the increased fraction of N in benthic organic matter, as shown by the organic C:N ratio (Fig. 3). Although the fraction of inorganic, particle bound nitrogen might be a concern when assessing TOC/TN ratios for the purpose of assessing vertical gradients in organic matter origin and lability (Schubert and Calvert, 2001), this is true for sediments of low organic and high clay + silt content (Stevenson and Dhariwal, 1959; Silva and Bremner, 1966). However, the fraction of clays and silts present in the sediments under study was very low (Section 4.1). Furthermore, a linear correlation between TN and TOC for our sediments shows a negative intercept for %TOC = 0 (%TN = $(0.023 \pm 0.0048) \times$ %TOC $- (0.0087 \pm 0.0045%)$, $n = 36$, $P<0.0001$), so we can confidently state that for the purpose of assessing organic matter quality, TN = TON in our sediments and the C:N ratio changes with depth are not a result of mobilization of NH_4^+ adsorbed by clays, but are instead due to changes in the composition of organic matter with depth. This way, marine organic matter introduced into the sandy beach face by tidal oscillation, wave run-up and drainage processes (Riedl et al., 1972; McLachlan, 1989; Jiao and Li, 2004) may contribute significantly to the modulation of benthic reactivity, and consequently to the transformation of SGD-borne nitrate, since the largest pore-water N concentration gradients are found on the first 10 cm of the sediment column, where benthic organic matter is significantly enriched in nitrogen compared to deeper layers. Thus, tidal oscillation might also control nitrate removal at the seepage face. However, dispersion linked to advection of porewater and convective mixing across the sediment–water interface might contribute to porewater depth profiles that are not purely a reflection of benthic reactivity. This is particularly true for the November experiment, where shorter intervals between profile samples were the norm (see high variability in the salinity profiles, for example, A2 – 19:00 and A5 – 7:00, Fig. 6).

The hypothesis whereby N transformation is occurring was tested with mixing diagrams on the profiles that did not show evidence of vertical mixing, thus all but profiles A2, B5 and B2, B5. The theoretical (due to mixing only) distribution of DIN (as $NO_3^- + NH_4^+ + NO_2^-$) within the sampled sediment profiles was calculated for the November time-series and compared with the measured gradients. A selection of these comparisons, evidencing the range of possible differences, is plotted in Fig. 10. This exercise shows that loss of nitrogen from the system happens often, particularly so at the lower

[DIN] (µmol dm^{-3})
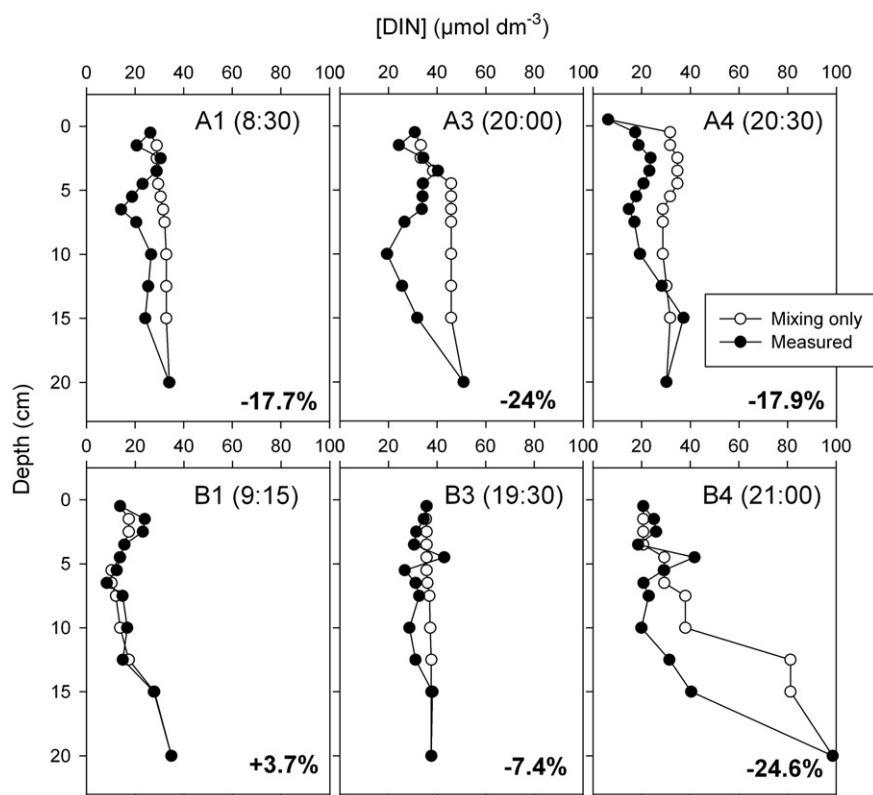
Fig. 10. Porewater mixing curves, depicting the concentrations of DIN ($NH_4^+ + NO_3^- + NO_2^-$) measured in depth (closed symbols), with the theoretical concentration profiles justified by mixing processes only (open symbols), for a selection of profiles collected at various stages of the tidal cycle during November 2005. Uppermost plots represent profiles taken at location A (upper seepage zone), whilst lowermost represent a selection of those collected at location B (lower seepage zone). Identification of the plots (A1, A2, B3, etc) follows the temporal sequence scheme in Fig. 6, for reference to the tidal stage. Numbers on the low right-hand side of each plot represent the relative loss of nitrogen from the system, calculated by the difference between the integrated areas of both curves. For discussion, see Section 5.3.

beach face (A1, A3, A4), and occasionally higher up (see B4). However, because the analysis rests on the assumption that flow is essentially directed upward, the potential role of horizontal advection in shaping the measured concentration depth gradients must be discussed. Shifts in the direction of flow could affect the analysis of the results based on mixing curves, because concentration gradients would be affected by lateral solute transfer, which would affect the vertical mixing gradients as shown in Fig. 10 and render the principle of vertical dilution moot. As a consequence, the implied differences attributed to reaction could potentially arise just on the strength of lateral flow and horizontal mixing.

Nevertheless, the experimental design, including the relative positions of the sampling devices (Fig. 2, upper panel) aimed to minimize the possibility of horizontal drainage affecting the results without a measure of control on whether it might be happening. In fact, the results lend credence to the assumption that seepage flow was essentially vertical at A and B. Firstly, the most important artefact negating this assumption would be substantial drainage of porewater through the upper beach levels (for example, water draining from station C into the areas occupied by station A and B) affecting solute concentrations and depth-gradients downslope. However, it is clearly demonstrated that the vertical distribution of porewater solutes in station C (above the seepage zone, Fig. 2) is completely different from what is observed downslope. Data from the profiler at station C revealed this difference throughout all sampling trips, and was thus eliminated from the plots, with the exception of November (Fig. 6, lower panel), which was used to make the point. The porewater salinity was always higher at C than at A and B, and did not change with depth or with tide levels (Fig. 6). Secondly, the vertical hydraulic conductivity in the sampled horizon (Fig. 3, panel on the right) suggests that if lateral flows were present, these would most certainly

occur preferentially through the surficial 0–8 cm layer, because the conductivity there was one order of magnitude higher than for the layers below. Whilst this seems a viable possibility in view of the distinct nitrogen solute behaviour in the surface layers at A and B in November (see Fig. 6, middle panels), when conceivably the recorded minima in N solute levels could be due to the carryover of nutrient-poor water from above, the salinity profiles do not support the notion. That can be verified by comparing salinities throughout the sediment column at station C (Fig. 6) with those measured at stations B and A: if porewater in the upper layers of the latter sites was advected from the former, the salinity gradients in the first few centimetres at sites A and B would be distinctively higher than what effectively was measured. Instead, we observed continuous salinity transitions, both in depth and in time, with the possible exceptions that were already mentioned, i.e., profiles A2, A5 and B5, which show salinity gradients more consistent with vertical convection than with horizontal transfer. Certainly, this potential misconception does not hold for the profiles collected in March, April and August, where the salinity profiles were almost uniform up to the sediment–water or air interface (Figs. 7 and 8), and the concentration peaks of both NO_3^- and NH_4^+ where quite evident near the surface. If lateral flow was important to define solute gradients at A and B in March, April and August, then the porewater levels of ammonium and nitrate at the lower stations would be diluted by water coming from above, and salinity would be higher, especially in the more conductive surface layers (Fig. 3). However, the invariance of the salinity profiles with depth at both levels, the maintenance of different asymptotic ranges in salinity (see for instance 22:05 B and 22:30 A, August, Fig. 8), and the fact that NO_3^- and NH_4^+ peaked at the surface in the lower stations support our contention that the direction of flow at A and B was essentially vertical. Finally, the wells covering the whole beach transect (Fig. 2) from which water representing a compositional

average of the first tens of centimetres of the beach section was collected, also showed a significant difference in porewater characteristics between the lower and the upper levels of the beach (Fig. 4). In addition, with the exception of well 1, located in the middle of the seepage zone (Fig. 2) the other wells (buried to ~40 cm, Section 3.1.1.) during ebb tide (Section 4.1) were dry, and profiler C (see Fig. 2, upper panel) was also located in dry sand when most of the profiles at A and B were sampled. This is visible in the timing of the profile sampling (Fig. 6, upper panel), because effectively, the presence or absence of water in well 2 was used to decide whether or not to sample from profiler C. Combined, these observations imply that there would be no significant hydraulic gradient on the beach driving lateral flow when SGD was most active, at least from the upper beach (see relative positions of sampling devices, Fig. 2, upper panel), supporting our assumption of vertical flow and reactivity in depth as the main drivers of the change in profile shape.

Consequently, if our assumption that the porewater flow largely occurs in the vertical sense is viable, it is clear that sediments at the seepage face modulate nitrogen fluxes into the lagoon, by supporting a measure of biogeochemical transformation of the groundwater-derived nitrate delivered by the oscillating intensity of SGD. Higher removal rates were associated with lower tide levels (see Fig. 6 for timing) and with lower position in the beach face. The depth integrated relative nitrate removal rates, expressed as a function of DIN introduced into the top 20 cm by seepage and averaged over the whole time-series, were $20.1 \pm 10.5\%$ for A and $4 \pm 5.9\%$ for B, thus suggesting that while net removal of nitrogen from the system occurs over the long run, periods when nitrogen is conserved or even amplified within the system are also observed, particularly at site B. Two features common to several profiles make the latter particularly evident: one is the prevalence of nitrate concentration peaks near the sediment surface, maintained against high seepage velocities (Figs. 6, 7–8), which suggests active nitrification during SGD. On the other hand, these are absent during high tide (for an example, see comparison between high and low tide profiles, August, Fig. 8). The other feature is rather less obvious, viz: superimposition of the NO_3^- and the NH_4^+ profiles, particularly those taken in November, suggests that some of the nitrate being transported into the upper layers of the sediment column might be reduced to ammonium, thus implying that Dissimilatory Nitrate Reduction to Ammonium (DNRA) might also be a feature of local biogeochemistry. Similar features, i.e., NO_3^- peaking at the surface and complementarities between nitrate and ammonium profiles, can be visible in March (A and B) and April (B). The potential for alternate N transformation pathways overlapping on small spatial scales is not novel and may actually have been masked in the past by a flawed view of the benthic N cycle (Zehr and Ward, 2002; Hulth et al., 2005; Burgin and Hamilton, 2007). The question therefore is whether, from our data, we can extract preliminary evidence of the co-occurrence of alternate oxidation–reduction N pathways.

5.4. Preliminary assessment of benthic NO_3^- reaction pathways

Albeit our knowledge of the N cycle is currently under revision (Zehr and Ward, 2002; Brandes et al., 2007), the accessibility and reactivity of organic matter, the availability of nitrate and, at least for Anammox, the co-occurrence of NH_4^+ and NO_2^- in the same benthic horizon are still understood to be key factors determining the extent and net rates of nitrate reduction/nitrogen removal in benthic systems (Herbert, 1999; Thamdrup and Dalsgaard, 2002). Understanding on whether the beach face might constitute a net sink, net source or a storage compartment for nutrients, and in particular, inorganic nitrogen, is a key factor underpinning awareness of the potential contribution of groundwater-borne nutrient loads into the coastal ecosystem (Hays and Ullman, 2007). In particular, the potential of the seepage face to attenuate nitrogen loading from land into the coastal ecosystem through denitrification and/or Anammox makes it a potential natural buffer constraining the effects of cultural eutrophication in SGD impacted systems. However, because of its central importance to benthic N redox reactions as an intermediate in canonical denitrification and nitrification, as well as being a key metabolite for Anammox, NO_2^- does not accumulate in substantive quantities in coastal porewaters, making it difficult to use the three solute forms of inorganic N (NH_4^+, NO_3^-, NO_2^-) in simple mass balance calculations. Superimposition of temporal and spatial dynamics of flow processes over the natural biogeochemical zonation at such sites further complicates the issue. However, given the evidence suggesting that at this site, flow through the surface sediment layers at the seepage face can be considered essentially vertical (see Section 5.3), we have taken the approach of calculating mass balances for NH_4^+ and NO_3^- in the spatial domain represented by the 20-cm deep slab of sediment sampled by the in-situ profilers. By assuming a local upward advective velocity equal to the average of the bulk seepage rates measured in-situ, and the concentrations of NH_4^+ and NO_3^- at the limits of the domain (i.e., at the sediment–water interface and at 20 cm depth) the rates of ammonium production (APR = $\Delta[NH_4^+]$), change of the nitrate pool (ΔNO_3^-), nitrate reduction (NRR = $-\Delta[NO_3^-]$) and net change of the DIN pool ($\Delta DIN = APR + \Delta NO_3^-$) were calculated for each profile, and then averaged for each site and month (Table 1). Concentration profiles with concomitant salinity gradients denouncing substantive mixing (standard deviation about the mean of all depths greater than 1%) were ignored for the purpose of this exercise. The objective was to carry out a preliminary assessment, when possible, of ratios of APR (Ammonium Production Rate) to NRR (Nitrate Reduction Rate), which have been successfully used to constrain the main pathways of nitrogen transformation in coastal sediments (Laverman et al., 2006, 2007). A cautionary note on this preliminary analysis is due, though: although we are using an average porewater velocity for each monthly set of profiles, and while this option might affect the actual figure obtained for

Table 1

Rates of ammonium production (APR = $\Delta[NH_4^+]$), change of the nitrate pool (ΔNO_3^-), nitrate reduction (NRR = $-\Delta[NO_3^-]$), net change of the DIN pool ($\Delta DIN = APR + \Delta NO_3^-$) and respective APR/NRR ratios ($\pm$ unbiased Standard Error of the mean) calculated for the domain represented by the vertical distance sampled for porewater concentration profiles (0 to 20 cm depth at the seepage face).

Month	N	U (cm h^{-1})	APR (mmol m^{-2} h^{-1} $\pm$ SE)	ΔNO_3^- (mmol m^{-2} h^{-1} $\pm$ SE)	APR/NRR ($\pm$ SE)	ΔDIN (mmol m^{-2} h^{-1} $\pm$ SE)
Nov A	4	22.0	0.82 ± 0.20	-2.34 ± 0.82	0.43 ± 0.14	-1.53 ± 0.80
Nov B	4	22.0	2.2 ± 0.55	-4.43 ± 1.43	0.66 ± 0.29	-2.23 ± 1.36
Mar A	4	7.7	0.08 ± 0.05	-0.81 ± 0.17	0.11 ± 0.07	-0.73 ± 0.17
Mar B	2	7.3	0.01 ± 0.01	0.05 ± 0.05	-0.08 ± 0.08	0.06 ± 0.06
Apri A	3	3.6	–	0.06 ± 0.03	–	0.06 ± 0.03
Apri B	3	5.1	0.001 ± 0.001	0.003 ± 0.02	0.31 ± 0.31	0.004 ± 0.02
Aug A	3	7.6	–	0.65 ± 0.20	–	0.65 ± 0.20
Aug A-HT	1	0.0	–	-0.07	–	-0.07
Aug B	3	4.8	–	0.31 ± 0.13	–	0.31 ± 0.13
Aug B-HT	1	0.0	–	-0.003	–	-0.003

Concentration profiles for which salinity gradients denounced substantive mixing (standard deviation about the mean of all depths greater than 1%) were ignored for the purpose of this exercise. Mean values were obtained by averaging results obtained for the mass balance calculation applied to each individual profile (n = number of profiles used in each calculation). U is the porewater velocity, extracted from seepage metering and benthic chamber area, averaged throughout the period of profile sampling, that was used for mass-balance calculations. "-HT" — suffix added to a profile taken during peak high tide. For extended discussion, see Section 5.4.

APRs and NRRs, the assumption does not affect the APR/NRR ratios themselves, nor does it affect the sign associated with each rate (i.e., choice of advective velocity does not affect findings related to either loss of the compound or gain of the compound within each layer). Thus, whilst the analysis might be improved for better reliance on the estimated rates per se, it is not the primary focus of this paper and will be subject of a forthcoming study. The highest rates of nitrate removal (0.81 ± 0.17 to 4.43 ± 1.43 mmol m^{-2} h^{-1}) were coupled to the highest rates of net ammonium production (0.08 ± 0.05 to 2.2 ± 0.55 mmol m^{-2} h^{-1}) in November and March A (mean APR $= -0.59 \times$ mean $\Delta NO_3^- - 0.45$, $R^2 = 0.993$, $P = 0.05$, $n = 3$), whilst March B, April and August were characterized by net nitrate production on average, generally coupled to low or undetectable net APRs. Nitrogen is lost from the system in November, March A and during high tide (August). When an increase in N is observed, it is mostly due to nitrification at the surface layer (Figs. 7 and 8). Although in November peak NH_4^+ concentrations are observed on the surface sediment layers, in all other occasions ammonium levels remain very low or below detection limits, making it difficult to rely on calculated APRs. Note however that although the net rates extracted from the mass balance approach are expressed on a per hour basis, they would only be applicable to a period of ~4 h a day, on account of the tidal modulation of seepage rate (see Section 5.1.) and the intrinsic dependence of reaction rates on the local porewater velocity in any reactive environment dominated by advection.

Although preliminary, this selection of mass balances is important to obtain indications of the reactive pathways involved in the transformation of groundwater-borne nitrate at the seepage face. For example, an analysis of Table 1 allows us to postulate that the nature of the system as a net source or sink for nitrogen will vary seasonally and with location on the beach cross-section; it also reveals that different processes might overlap, inducing both level and profile gradient changes as nitrate-laden porewater seeps through the decreasing C:N gradient to the sediment surface. Taking the C:N ratio of fresh phytoplankton (i.e., the Redfield ratio, C:N = 6.6), the theoretical APR/NRR ratio characteristic of heterotrophic denitrification would range from 0.17 to 0.19; this value decreases with diminishing reactivity of benthic organic matter. For example, for the C:N ratio of ~43 found in the deeper layers of our site (Fig. 3), the quotient would be ~0.03 instead. The average APR/NRR ratios determined for the whole domain, when net nitrate removal occurred (November, March A) ranged from 0.11 to 0.66 (Table 1). Whilst in March, the average APR/NRR ratio was found within the range characteristic of canonical denitrification, in November the average APR/NRR ratios where much higher (Table 1) thus suggesting alternate nitrate reduction processes, the likely candidate being DNRA. Assuming the Redfield ratio, the theoretical APR/NRR for DNRA would be 1.3. However, due to the compositional ratio of organic matter with depth (Fig. 3) this would range from 1.13 in the topmost sediment layer (C:N = 15) to 1.04 in the deeper 10–20 cm of our site. The intermediate values found instead suggest that DNRA and heterotrophic denitrification co-occur, as already postulated for estuarine sediments (KellyGerreyn et al., 2001) and suggested for coastal sediments (Laverman et al., 2006).

6. Conclusions

Our results show that the tide is a major controlling force over timing and magnitude of submarine groundwater discharge (SGD) in the Ria Formosa. The resultant intermittent outflow of brackish water, in phase with the low tide, contributes to nitrogen loading of the lagoon. Daily water renovation coefficients in the shallow lagoon (80% in spring and 50% in neap tides), combined with the impact of the tidal amplitude on the land-based hydraulic gradient driving SGD suggest that the freshwater component of discharge will decrease from spring to neap tides.

The harmonic pumping of SGD-borne nitrate into the seepage face from below, in response to the lowering of water pressure when tidal levels drop, affects local benthic nitrogen biogeochemistry. Analysis of

mixing curves constructed from in-situ profiles of porewater DIN levels and salinity showed that biogeochemical reactions controlling NH_4^+ and NO_3^- concentrations within the first 20 cm layer of the seepage face were faster than dispersion effects created by mixing. Still, the most significant changes to inorganic nitrogen concentrations and speciation coincide with a strong depth-gradient in bulk organic matter quality, as perceived by the C:N ratio (from 15 to 43 over 20 cm). Hence, the rhythmic pumping of brackish, nitrate bearing porewaters into the surficial layers of the sediment might also exert significant control over both the net rates of nitrogen transformation and the prevailing benthic reaction pathways.

Mass budgets of the inputs and outputs of NH_4^+ and NO_3^- across the sampled sediment were executed on profile sets collected in November 2005 ($n = 8$), March ($n = 6$), April ($n = 6$) and August 2006 ($n = 6$), whereupon net rates of N transformation were obtained. These revealed that net attenuation of N loading into the lagoon occurred in November (-1.53 ± 0.8 and -2.23 ± 1.36 mmol N m^{-2} h^{-1} respectively at the lower and upper reaches of the seepage face) and March at the lower end of the seepage zone (-0.73 ± 0.17 mmol N m^{-2} h^{-1}).

However, net SGD-borne N flux was enhanced throughout the remainder of the sampling periods. Although the benthic environment at the seepage face seems, occasionally (e.g. November 2005), to attenuate the groundwater-borne DIN loading of the lagoon, a preliminary mass balance analysis, coupled to stoichiometric calculations based on the ratio of net ammonium production to nitrate reduction rates, suggests that a proportion of the nitrogen being transported through the seepage face by SGD may be transformed through dissimilatory nitrate reduction to ammonium (DNRA), and that nitrification may add to the nitrate flowing into the lagoon. Notwithstanding the simplicity of the approach, net APRs and NRRs suggest that co-occurrence of different nitrate reduction pathways (e.g. incomplete denitrification and DNRA) over small spatial scales can be characteristic of beach faces locus of SGD. Whilst better net rate and reactive length estimates might be drawn from modelling aids, particularly the use of analytical Advective Dispersion Reaction models describing porewater nitrate depth gradients that would allow segregation of the dispersive effects from the reactive influence over profile shape, microbial community analysis coupled to isotope pairing studies in field and lab settings are needed to clarify the extent and relative importance of differential pathways of N transformation at beach faces harbouring SGD.

Acknowledgements

References

Almeida, C., Silva, M.L., 1987. Incidence of agriculture on water quality at Campina de Faro (South Portugal). Hidrogeologia-y-Recursos-Hidraulicos, vol. 12. Associacion Española de Hidrologia Subterranea, Madrid, Spain, pp. 249–257.

Almeida, C.J., Mendonca, J.J.L., Jesus, M.R., Gomes, A.J., 2000. Sistemas aquiferos de Portugal Continental [Aquifer Systems of Continental Portugal]. Instituto Nacional da Água-INAG. (Portuguese).

Andrade, C., Freitas, M.C., Moreno, J., Craveiro, S.C., 2004. Stratigraphical evidence of Late Holocene barrier breaching and extreme storms in lagoonal sediments of Ria Formosa, Algarve, Portugal. Mar. Geol. 210, 339–362.

Arnaud-Fassetta, G., Bertrand, F., Costa, S., Davidson, R., 2006. The western lagoon marshes of the Ria Formosa (Southern Portugal): sediment–vegetation dynamics, long-term to short-term changes and perspective. Cont. Shelf Res. 26, 363–384.

Ataie-Ashtiani, B., Volker, R.E., Lockington, D.A., 2001. Tidal effects on groundwater dynamics in unconfined aquifers. Hydrol. Process. 15, 655–669.

Balouin, Y. Les embouchures mésotidales (tidal inlets) et leur relation avec les littoraux adjacents − Exemple de la Barra Nova, Sud Portugal [PhD thesis]. University of Bordeaux; 2001. French.

Bettencourt, P. Les Environnements Sedimentaires de la Cote Sotavento (Algarve, Sud Portugal) et leur Evolution Holocene et Actuelle [PhD thesis]. University of Bordeaux; 1994. French.

Bokuniewicz, H., Pavlik, B., 1999. Groundwater seepage along a Barrier Island. Biodegradation 10, 257–276.

Bokuniewicz, H.J., 1992. Analytical descriptions of subaqueous groundwater seepage. Estuaries 15, 458–464.

Bokuniewicz, H.J., Buddemeier, R., Maxwell, B., Smith, C., 2003. The typological approach to submarine groundwater discharge (SGD). Biogeochemistry 66, 145–158.

Bonte, M. A chemical and isotopic study after the hydrogeochemical processes occurring under irrigated land in Campina da Luz, Algarve, Portugal [MsC dissertation]. Free University of Amsterdam; 1999.

Boski, T., Moura, D., Veiga-Pires, C., Camacho, S., Duarte, D., Scott, D.B., et al., 2002. Postglacial sea-level rise and sedimentary response in the Guadiana Estuary, Portugal/Spain border. Sediment. Geol. 150, 103–122.

Bowen, J., Kroeger, K., Tomasky, G., Pabich, W., Cole, M., Carmichael, R., et al., 2007. A review of land-sea coupling by groundwater discharge of nitrogen to New England estuaries: mechanisms and effects. Appl. Geochem. 22, 175–191.

Brandes, J., Devol, A., Deutsch, C., 2007. New developments in the marine nitrogen cycle. Chem. Rev. 107, 577–589.

Burgin, A.J., Hamilton, S.K., 2007. Have we overemphasized the role of denitrification in aquatic ecosystems? A review of nitrate removal pathways. Front. Ecol. Environ. 5, 89–96.

Burnett, W.C., Taniguchi, M., Oberdorfer, J., 2001. Measurement and significance of the direct discharge of groundwater into the coastal zone. J. Sea Res. 46, 109–116.

Burnett, W.C., Bokuniewicz, H., Huettel, M., Moore, W.S., Taniguchi, M., 2003. Groundwater and pore water inputs to the coastal zone. Biogeochemistry 66, 3–33.

Cable, J., Burnett, W., Chanton, J., Corbett, D., Cable, P., 1997. Field evaluation of seepage meters in the coastal marine environment. Estuar. Coast. Shelf Sci. 45, 367–375.

Cappuyns, V., Swennen, R., Devivier, A., 2004. Influence of ripening on pHstat leaching behaviour of heavy metals from dredged sediments. J. Environ. Monit. 6, 774–781.

Capone, D.G., Bautista, M.F., 1985. A groundwater source of nitrate in nearshore marine sediments. Nature 313, 214–216.

Cardwell, W.T., Parsons, R.I., 1945. Average permeability of heterogeneous sands. Trans. Am. Inst. Min. Eng. 160, 34–42.

Carruthers, T., van Tussenbroek, B., Dennison, W., 2005. Influence of submarine springs and wastewater on nutrient dynamics of Caribbean seagrass meadows. Estuar. Coast. Shelf Sci. 64, 191–199.

Chanton, J.P., Burnett, W.C., Dulaiova, H., Corbett, D.R., Taniguchi, M., 2003. Seepage rate variability in Florida Bay driven by Atlantic tidal height. Biogeochemistry 66, 187–202.

Charette, M.A., 2007. Hydrologic forcing of submarine groundwater discharge: insight from a seasonal study of radium isotopes in a groundwater-dominated salt marsh estuary. Limnol. Oceanogr. 52, 230–239.

Charette, M.A., Sholkovitz, E.R., Hansel, C.M., 2005. Trace element cycling in a subterranean estuary: part 1. Geochemistry of the permeable sediments. Geochim. Cosmochim. Acta 69, 2095–2109.

Charette, M.A., Sholkovitz, E.R., 2006. Trace element cycling in a subterranean estuary: part 2. Geochemistry of the pore water. Geochim. Cosmochim. Acta 70, 811–826.

Chester, D.K., James, P.A., 1995. The Pleistocene Faro/Quarteira formation of the Algarve region, southern Portugal. Geomorphology 12, 133–149.

Corbett, D., Chanton, J., Burnett, W., Dillon, K., Rutkowski, C., Fourqurean, J., 1999. Patterns of groundwater discharge into Florida Bay. Limnol. Oceanogr. 44, 1045–1055.

Dalsgaard, T., Thamdrup, B., 2002. Factors controlling anaerobic ammonium oxidation with nitrite in marine sediments. Appl. Environ. Microbiol. 68, 3802–3808.

Dias, J.M.A., Boski, T., Rodrigues, A., Magalhães, F., 2000. Coast line evolution in Portugal since the Last Glacial Maximum until present − a synthesis. Mar. Geol. 170, 177–186.

Grasshoff, K., Ehrhardt, M., Kremling, K., 1999. Methods of Seawater Analysis, 3rd Ed. Wiley-VCH, Weinheim, Germany.

Hays, R., Ullman, W., 2007. Dissolved nutrient fluxes through a sandy estuarine beachface (Cape Henlopen, Delaware, U.S.A.): contributions from fresh groundwater discharge, seawater recycling, and diagenesis. Estuar. Coasts 30, 710–724.

Herbert, R.A., 1999. Nitrogen cycling in coastal marine ecosystems. FEMS Microbiol. Rev. 23, 563–590.

Hidrografico, I. Marés 81/82 Ria de Faro. Estudo das marés de oito estações da Ria de Faro. Lisbon: IH-Instituto Hidrografico (Rel. FT-MC-4/86); 1986.

Hirota, J., Szyper, J.P., 1975. Separation of total particulate carbon into inorganic and organic components. Limnol. Oceanogr. 20, 896–900.

Hulth, S., Aller, R.C., Canfield, D.E., Dalsgaard, T., Engström, P., Gilbert, F., et al., 2005. Nitrogen removal in marine environments: recent findings and future research challenges. Mar. Chem. 94, 125–145.

Jiao, J.J., Li, H., 2004. Breathing of coastal vadose zone induced by sea level fluctuations. Geophys. Res. Lett. 31, L11502.

Johannes, R.E., 1980. The ecological significance of the submarine discharge of ground-water. Mar. Ecol., Prog. Ser. 3, 365–373.

Jones, M.N., 1984. Nitrate reduction by shaking with cadmium: alternative to cadmium columns. Water Res. 18, 643–646.

KellyGerreyn, B.A., Trimmer, M., Hydes, D.J., 2001. A diagenetic model discriminating denitrification and dissimilatory nitrate reduction to ammonium in a temperate estuarine sediment. Mar. Ecol., Prog. Ser. 220, 33–46.

Kim, G., Ryu, J., Yang, H., Yun, S., 2005. Submarine groundwater discharge (SGD) into the Yellow Sea revealed by 228Ra and 226Ra isotopes: implications for global silicate fluxes. Earth Planet. Sci. Lett. 237, 156–166.

Kjervfe, B. (Ed.), 1994. Coastal Lagoon Processes. InElsevier, Amsterdam.

Laverman, A.M., Van Cappellen, P., Van Rotterdam-Los, D., Pallud, C., Abell, J., 2006. Potential rates and pathways of microbial nitrate reduction in coastal sediments. FEMS Microbiol. Ecol. 58, 179–192.

Laverman, A.M., Canavan, R.W., Slomp, C.P., Cappellen, P.V., 2007. Potential nitrate removal in a coastal freshwater sediment (Haringvliet Lake, The Netherlands) and response to salinization. Water Res. 41, 3061–3068.

Lee, D., 1977. A device for measuring seepage flux in lakes and estuaries. Limnol. Oceanogr. 22, 140–147.

Leote, C., Ibánhez, J., Rocha, C., 2008. Submarine Groundwater Discharge as a nitrogen source to the Ria Formosa studied with seepage meters. Biogeochemistry 88, 185–194.

Luo, Y., Qiao, X., Song, J., Christie, P., Wong, M., 2003. Use of a multi-layer column device for study on leachability of nitrate in sludge-amended soils. Chemosphere 52, 1483–1488.

McLachlan, A., 1989. Water filtration by dissipative beaches. Limnol. Oceanogr. 34, 774–780.

Mackenzie, F.T., Ver, L.M., Lerman, A., 2002. Century-scale nitrogen and phosphorus controls of the carbon cycle. Chem. Geol. 190, 13–32.

Moore, W.S., 1999. The subterranean estuary: a reaction zone of ground water and sea water. Mar. Chem. 65, 111–125.

Moore, W.S., 2006. The role of submarine groundwater discharge in coastal biogeochemistry. J. Geochem. Explor. 88, 389–393.

Moore, W.S., Wilson, A.M., 2005. Advective flow through the upper continental shelf driven by storms, buoyancy, and submarine groundwater discharge. Earth Planet. Sci. Lett. 235, 564–576.

Paerl, H.W., 1999. Cultural eutrophication of shallow coastal waters: coupling changing anthropogenic nutrient inputs to regional management approaches. Limnologica 29, 249–254.

Paulsen, R.J., O'rourke, D., Smith, C.F., Wong, T., 2004. Tidal load and salt water influences on submarine ground water discharge. Ground Water 42, 990–999.

Riedl, R.J., Huang, N., Machan, R., 1972. The subtidal pump: a mechanism of interstitial water exchange by wave action. Mar. Biol. 13, 210–221.

Robinson, M.A., Gallagher, D.L., Reay, W., 1998. Field observations of tidal and seasonal variations in ground water discharge to tidal estuarine surface water. Ground Water Monit. Remediat. 18, 83–92.

Robinson, M.A., Gallagher, D.L., 1999. A model of ground water discharge from an unconfined coastal aquifer. Ground Water 37, 80–87.

Rocha, C., Forster, S., Koning, E., Epping, E., 2005. High-resolution permeability determination and two-dimensional pore water flow in sandy sediment. Limnol. Oceanogr. Meth. 3, 10–23.

Salles, P. Hydrodynamic controls on multiple tidal inlet persistence [PhD Thesis]. Massachusetts Institute of Technology and Woods Hole Oceanographic Institution Joint Program in Oceanography/Applied Ocean Science and Engineering; 2001.

Schubert, C.J., Calvert, S.E., 2001. Nitrogen and carbon isotopic composition of marine and terrestrial organic matter in Arctic Ocean sediments: implications for nutrient utilization and organic matter composition. Deep-Sea Res., Part 1, Oceanogr. Res. Pap. 48, 789–810.

Seabra de Melo, J.L.B., 1989. Caracterizacao hidro-oceanografica da Ria Formosa, vol. 10. Anais do Instituto Hidrográfico, pp. 7–23 (Portuguese).

Seeberg-Elverfeldt, J., Schluter, M., Feseker, T., Kolling, M., 2005. Rhizon sampling of pore waters near the sediment–water interface of aquatic systems. Limnol. Oceanogr. Meth. 3, 361–371.

Shaw, R., Prepas, E., 1989. Anomalous, short-term influx of water into seepage meters. Limnol. Oceanogr. 34, 1343–1351.

Silva, J.A., Bremner, J.M., 1966. Determination and isotope ratio analysis of different forms of nitrogen in soils. 5. Fixed ammonium. Soil Sci. Soc. Am. Proc. 30, 587–594.

Slomp, C.P., Van Cappellen, P., 2004. Nutrient inputs to the coastal ocean through submarine groundwater discharge: controls and potential impact. J. Hydrol. 295, 64–86.

SNIRH/INAG, 2008. Águas Subterrâneas (Dados Sintetizados) [Internet]. [cited 2008 Sep 1] Available from: http://snirh.inag.pt/snirh/dados_sintese/agsub/pontosa-gua/site/entrada.php?uh=M&sa=M12-CAMPINA_DE_FARO.

Song, J., Luo, Y.M., Zhao, Q.G., Christie, P., 2003. Novel use of soil moisture samplers for studies on anaerobic ammonium fluxes across lake sediment–water interfaces. Chemosphere 50, 711–715.

Stevenson, F.J., Dhariwal, A.P.S., 1959. Distribution of fixed ammonium in soils. Soil Sci. Soc. Am. Proc. 23, 121–125.

Stigter, T.Y., van Ooijen, S.P.J., Post, V.E.A., Appelo, C.A.J., Carvalho Dill, A.M.M., 1998. A hydrogeological and hydrochemical explanation of the groundwater composition under irrigated land in a Mediterranean environment, Algarve, Portugal. J. Hydrol. 208, 262–279.

Stigter, T., Carvalho Dill, A., Ribeiro, L., Reis, E., 2006. Impact of the shift from groundwater to surface water irrigation on aquifer dynamics and hydrochemistry in a semi-arid region in the south of Portugal. Agric. Water Manag. 85, 121–132.

Taniguchi, M., 2002. Tidal effects on submarine groundwater discharge into the ocean. Geophys. Res. Lett. 29, 1561.

Taniguchi, M., Iwakawa, H., 2004. Submarine groundwater discharge in Osaka Bay, Japan. Limnology 5, 25–32.

Taniguchi, M., Burnett, W.C., Smith, C.F., Paulsen, R.J., O'Rourke, D., Krupa, S.L., et al., 2003. Spatial and temporal distributions of submarine groundwater discharge rates obtained from various types of seepage meters at a site in the Northeastern Gulf of Mexico. Biogeochemistry 66, 35–53.

Thamdrup, B., Dalsgaard, T., 2002. Production of N_2 through anaerobic ammonium oxidation coupled to nitrate reduction in marine sediments. Appl. Environ. Microbiol. 68, 1312–1318.

Turner, I.L., 1998. Monitoring groundwater dynamics in the littoral zone at seasonal, storm, tide and swash frequencies. Coast. Eng. 35, 1–16.

Uchiyama, Y., Nadaoka, K., Rölke, P., Adachi, K., Yagi, H., 2000. Submarine groundwater discharge into the sea and associated nutrient transport in a sandy beach. Water Resour. Res. 36, 1467–1479.

Ullman, W.J., Chang, B., Miller, D.C., Madsen, J.A., 2003. Groundwater mixing, nutrient diagenesis, and discharges across a sandy beachface, Cape Henlopen, Delaware (USA). Estuar. Coast. Shelf Sci. 57, 539–552.

Urish, D.W., Mckenna, T.E., 2004. Tidal effects on ground water discharge through a sandy marine beach. Ground Water 42, 971–982.

Valiela, I., 1992. Coupling of watersheds and coastal waters: an introduction to the dedicated issue. Estuar. Coasts 15 (4), 429–430.

Valiela, I., Foreman, K., LaMontagne, M., Hersh, D., Costa, J., Peckol, P., et al., 1992. Couplings of watersheds and coastal waters: sources and consequences of nutrient enrichment in Waquoit Bay, Massachusetts. Estuaries 15 (4), 443–457.

Valiela, I., Costa, J., Foreman, K., Teal, J., Howes, B., Aubrey, D., 1999. Transport of groundwater-borne nutrients from watersheds and their effects on coastal waters. Biodegradation 10 (3), 177–197.

Verhoeven, J.T., Arheimer, B., Yin, C., Hefting, M.M., 2006. Regional and global concerns over wetlands and water quality. Trends Ecol. Evol. 21, 96–103.

Vila-Concejo, A., Ferreira, Ó., Matias, A., Dias, J.M.A., 2003. The first two years of an inlet: sedimentary dynamics. Cont. Shelf Res. 23, 1425–1445.

Vila-Concejo, A., Ferreira, Ó., Morris, B., Matias, A., Dias, J., 2004. Lessons from inlet relocation: examples from Southern Portugal. Coast. Eng. 51, 967–990.

Vitousek, P.M., Mooney, H.A., Lubchenco, J., Melillo, J.M., 1997. Human domination of Earth's ecosystems. Science 277, 494–499.

Wentworth, C.K., 1922. A scale of grade and class terms for clastic sediments. J. Geol. XXX, 377–392.

Zehr, J.P., Ward, B.B., 2002. Nitrogen cycling in the ocean: new perspectives on processes and paradigms. Appl. Environ. Microbiol. 68, 1015–1024.